Summer 2016

Small Molecule Disruption of ROS-Regulating Pathways in Human Carcinoma

Rebecca E. McCall

SMALL MOLECULE DISRUPTION OF R.O.S.-REGULATING PATHWAYS IN HUMAN CARCINOMA

by

REBECCA M^{C}CALL

(Under the Direction of Jonathan F. Arambula)

Abstract

Gold (I) coordinated N-heterocyclic carbenes containing appended redox cycling moieties were designed and analyzed for their ability to target the antioxidant network via multiple mechanisms in various human cancer cell models. Complexes containing either ferrocene or naphthoquinone redox cycling moieties were screened for inhibition of cell growth, inhibition of thioredoxin reductase (TrxR), and accentuation of exogenous ROS. The cell death pathway employed was determined by flow cytometry via detection of Annexin-V FITC. Furthermore, differential gene expression between treated cells and untreated cells revealed the induction of endoplasmic reticulum stress and unfolded protein response pathways.

Index words: Cancer, ROS, A549, A2780, A2780CP, PC-3, Gold, Inorganic medicinal chemistry, Drug development

SMALL MOLECULE DISRUPTION OF R.O.S.-REGULATING PATHWAYS IN HUMAN CARCINOMA

by

REBECCA M^{C}CALL

B.S., Georgia Southern University, 2014

A Thesis Submitted to the Graduate Faculty of Georgia Southern University in

Partial Fulfillment of the Requirements for the Degree

MASTER OF SCIENCE

STATESBORO, GEORGIA

SMALL MOLECULE DISRUPTION OF R.O.S.-REGULATING PATHWAYS IN HUMAN CARCINOMA

by

REBECCA M^{C}CALL

Major Professor: Jonathan F. Arambula

Committee: Worlanyo Eric Gato

Amanda Stewart

Electronic Version Approved:

July 2016

Dedication

For Kandi Adams Beckum

Acknowledgements

For the following assistance and contributions, the author would like to acknowledge:

Dr. Arambula, for being my research advisor and generally putting up with my crazy.

The other members of the Arambula lab, Briana Burney, Zarana Patel, Alex Rodriguez, Kamaree Harris, Connor Bizon, Maggie Seckman, Cristy York, Mila Flores, Tori Hicks, Chad Burleson, and Jose Ruiz. They also put up with a good deal of crazy, and some worked on this project with me.

Dr. Kuppuswamy Arumugam, for synthesizing and co-designing the compounds for study.

Dr. Kocerha, for her help with RNA extraction, PCR, and ICP-MS.

Dr. Stewart, for letting me hang out in her lab and borrow her keys as necessary. Also, thanks for agreeing to be on my thesis committee.

Dr. Gato, for letting us use his Modified Lowry kit and his RNA extraction kit, as well as his thermal cyclers and cute centrifuges. Also, thanks for agreeing to be on my thesis committee.

Dr. Stone, for allowing us to use his Trace Metal Grade HCl.

Dr. Aiken, for giving us zinc acetate and gold (I) chloride instead of making us buy our own.

Dr. Abid and Dr. Sittaramane for their collaboration and the papers that have resulted from it.

The other graduate students, also for unlocking doors and being there to satisfy safety requirements at odd hours and over weekends (in no particular order: Chad Burleson, Stephanie Canonico-May, Domonique Winder, Amanda Murawski, Aimee Lorts, Matt Bassett, Simpo Rose Akech).

Ms. Kathy Gay, Mr. Thomas Anderson, Mrs. Drew Callaway, and the Nursing/Chemistry Building janitorial staff, for helping with logistical issues.

Contents

List of Tables

List of Figures

Chapter 1. Introduction

1.1 Network Pharmacology

Traditionally, new medications are designed to target a single gene or protein in the body. The idea is that by designing a small molecule to only interact with a single target, the potential side effects of the drug will be minimized. While these drugs can be effective for a time, they are usually limited to a single mechanism of action by their single target. Often, single target inhibition fails to alter phenotypic response due to signal redirection (Figure 1b). This adaptation

is problematic in anti-cancer therapy. When anticancer therapeutics have a single target, cancer cells can become resistant to the drug.[1–3] In the clinic, the patient will then need higher doses to maintain the efficacy of the drug, or a new drug altogether. The second approach is problematic because there may not be another effective drug for the particular form of cancer in existence. However, a drug that targets multiple points along a pathway, instead of a single point, may work by multiple mechanisms (Figure 1c). This combination approach may overwhelm the target pathway and lead to greater alterations of the target phenotype, in addition to potentially reducing resistance, as the cells would have to develop resistance mechanisms for all of the mechanisms that the multimodal drug employs. We hypothesize that multimodal pathway targeting will result in phenotypic alterations that are controlled by said pathway. The antioxidant pathway was used as a model to test this hypothesis as it is a major intracellular defense pathway that is overexpressed in multiple cancers.

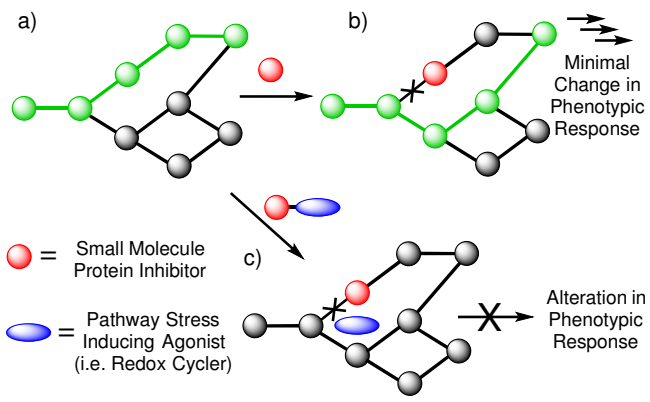

Figure 1. Illustration regarding bimodal network targeting. a) Normal (green) signal transduction within a generic biological network. b) In the presence of a small molecule protein inhibitor, the current pathway is shut down; however no change in response is observed due to redirection of the signal transduction. c) It is hypothesized that biochemical targeting with the same protein inhibitor in conjunction with a small molecule capable of inducing general pathway stress (i.e. redox cycler) will shut down the network, resulting in a greater alteration of the phenotypic response.

1.2 The Antioxidant Pathway

A mainstay in scientific education is an understanding of a biological system's constant struggle to achieve homeostasis. The idea of homeostasis is that there are certain substances that are necessary for cells to live and function properly, and the cells need to have certain amounts of these substances. Vitamins, nutrients, enzymes, antioxidants, and scavengers are all examples of such Biologically Relevant Entities (BRE). If a cell does not have enough of a BRE, we call that a deficiency. An excess of a BRE leads to an overabundance. The functional range of a BRE lies between both extremes and provides the ideal concentration for proper biological function. In certain contexts, an inability to achieve cellular homeostasis may result in altered growth mechanisms or cell death. However, cancer progression and tumorigenesis have often been ascribed to cellular adaptations of such homeostatic alterations induced by external sources (Figure 2). This is the result of constant cellular alterations of BRE concentrations to maintain the functional range of that substance.

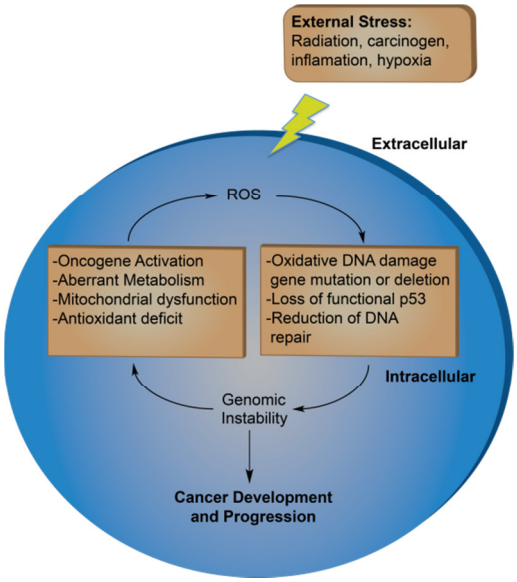

Figure 2. Examples of stresses and responses in cells related to cancer progression and tumorigenesis.

Reactive Oxygen Species (ROS) are byproducts of normal cellular metabolism. They are generally small molecules with unpaired electrons (also known as free radicals) on oxygen atoms within the molecule. Free radicals are highly reactive, so the presence of ROS is very dangerous for the cell. Oxidation of lipids and fatty acids by ROS often result in cell membrane destruction.[4–6] However, ROS are necessary for normal cell growth, as they play significant roles in iron homeostasis, anti-inflammatory pathways, and cell differentiation and proliferation.[5,7] This highlights the significance of the functional range for intracellular ROS. An overabundance of intracellular ROS is known as oxidative stress. This is important because oxidative stress is a common mode of toxicity in cells.[4]

The upper threshold on the functional range for ROS (between the functional range and oxidative stress) is maintained by antioxidant activity. Antioxidants are enzymes and small

molecules which act as reducing agents for reactive oxygen species. This neutralizes the threat posed to the cell by excessive ROS. Some known antioxidants include Vitamin C, Vitamin E, glutathione, superoxide dismutases (SODs), and thioredoxin.[4,6] Thioredoxin is found in almost all living things. It is known to reduce ROS directly as well as regenerate several other antioxidants found in the cell. Thioredoxin itself is regenerated by the enzyme thioredoxin reductase (TrxR), which together form the thioredoxin system of antioxidant activity. Thioredoxin reductase is also known to reduce multiple targets and regenerate multiple antioxidants. While most antioxidants, including thioredoxin, utilize thiol-sulfhydryl chemistry for redox maintenance of ROS, thioredoxin reductase utilizes both cysteine and selenocysteine residues in its active site.[6,8,9]

There are 3 distinct human thioredoxin systems. Trx-1 and TrxR1 are found in the cytoplasm of most human cells. Trx-2 and TrxR2 are found in the mitochondria of human cells. SpTrx and TrxR3 (now renamed TGR) are found in human spermatozoa.[6] Interestingly, TGR reduces both Trx and glutathione, hence the new name. Inhibition of Trx1 is generally therapeutic for those with arthritis. Inhibition of the mitochondrial thioredoxin system is lethal to cells.[8,9] The thioredoxin system is known to be overexpressed in cancer cells.[10–12]

1.3 Targeting of the Antioxidant Pathway

It has long been known that platinum-containing compounds, arsenic-containing compounds, gold (I) compounds, and quinone-containing compounds[13,14] inhibit the activity of thioredoxin reductase.[6] Several gold (I) phosphines have been shown to have therapeutic value due to their binding with intracellular protein targets, including TrxR.[8,9] This is done by ionic interactions with the selenocysteine residues in the active site of the enzyme. By introducing gold (I) N-heterocyclic carbenes to cells, TrxR activity can be significantly diminished. This lowers the threshold between oxidative stress and the functional range of reactive oxygen species in the cell. Prolonged exposure to gold (I) N-heterocyclic carbenes is toxic to cancer cells.

Another mechanism used in modulation of ROS-regulated pathways is introducing ROS-generating substances to the cells. Ferrocene has been studied for decades for this purpose. The iron core of a ferrocene has an oxidation state of 2^+. It can undergo the Fenton reaction with hydrogen peroxide (a common intracellular reactive oxygen species) to produce hydroxyl

radical(s) and ferrocenium. In the presence of reducing species, such as NADH or NADPH, the iron 3^+ of the ferrocenium can then be reduced to iron 2^+ to regenerate the ferrocene. Another redox-active functionality that can be used to generate intracellular ROS is quinone. Quinones can undergo one-electron redox reactions, forming a semi-quinone in the process, or two-electron redox reactions, forming hydroquinone. This is especially interesting from a pharmacological standpoint because quinones are biologically active and are already found throughout the cell. Common intracellular quinone-containing compounds include all forms of Vitamin K, Coenzyme Q (ubiquinone), and plastoquinone. We hypothesize that a single molecule capable of 1) reducing intracellular antioxidants via protein inhibition and 2) accentuating oxidative stress via redox cycling will disrupt ROS homeostasis via multiple mechanisms and result in alterations of growth stress phenotypes.

1.4 Cell Models Utilized

There are many cell lines that can be used for evaluation of the toxicological effects of compounds. The cell lines employed by the Arambula group are A549, A2780, A2780CP, and PC-3. The Arambula group works primarily with A549 because it is well-suited for studying intracellular ROS homeostasis.

The A549 cell line was established by D.J. Giard et al. in 1972, using epithelial cells from a lung carcinoma. The patient the cells came from was a 58-year-old Caucasian man. The cells have a doubling time of about 22 hours and can be transfected. A549 cells are not identical, and usually have 64-67 chromosomes.[15] They can have multiple copies of the X and/or Y chromosome or even absence of the Y chromosome.[16] This is significant because a healthy, normal human cell should have 46 chromosomes, of which there will be two X chromosomes, or one X and one Y. Because these cells came from a man, it is expected that they would have one X chromosome and one Y chromosome each. The A549 cell line is known to be tumorigenic, which means that these cells can form a tumor if injected into an organism.[17] Because these cells are from lung tissue, they have an elevated tolerance for intracellular ROS. A549 is known to overexpress the antioxidant thioredoxin reductase relative to normal cells.[10,12] For this reason, A549 is a good model to use when studying intracellular ROS levels and TrxR activity. This cell line is wild-type for the p53 tumor suppressor gene.[18]

The A2780 cell line was established by T. H. Ward in 1984 from an ovarian epithelial adenocarcinoma. It has a doubling time of 24 hours. It is also very easy to kill these cells because the patient from which it was derived had never undergone any anticancer treatment at the time. Two treatment-resistant lines were derived from this line (A2780CP and A2780ADR) by treating the cells with common chemotherapeutics for several consecutive passages. A2780CP is resistant to cisplatin, and has a doubling time of 48 hours. These cells require patience. A2780 and A2780CP are not available through the ATCC.[19–23] Our cells are from the M. D. Anderson Cancer Center, courtesy of Dr. Zahid Siddik and Dr. Guangan He. Also, they are both wild-type for the p53 gene.[18]

The PC-3 cell line was established by M.E. Kaighn et al. in 1979. The cells that were used were from prostate cancer that had metastasized to the nearby bone. PC-3 cells are epithelial cells from that bone, and the tumor was a grade 4 adenocarcinoma. The patient was a 62-year-old Caucasian male. PC-3 can be transfected, and has a doubling time of about 25 hours. It is tumorigenic, which means that when these cells are injected into mice, they form tumors (PC-3 happens to form tumors 100% of the time, reportedly). This is important to note, because some researchers have erroneously thought that only males need to be concerned about incidents involving PC-3. The fact that it metastasized to bone suggests that the cell line is in fact hazardous to anyone who has bones. These cells have about 62 chromosomes, and none of them have an identifiable Y chromosome.[24] PC-3 does not have a functional p53 gene.[18]

1.5 Previous Work

In an effort to determine whether both paradigms for modulating intracellular ROS levels could be utilized by a single molecule, several compounds were co-designed by Dr. Arambula and Dr. Kuppuswamy Arumugam. The first three compounds under the numbering system used were imidazolium salts, which were synthesized in the Arumugam lab according to literature procedures,[25–31] and used as precursors in the synthesis of all other compounds in the library. Compound **1** is an N-heterocyclic carbene. Compound **2** is an N-heterocyclic carbene with one ferrocene per molecule. Compound **3** has two ferrocenes per molecule appended to the N-heterocyclic carbene core. Compounds **4-7** are generally referred to as the first generation of compounds in this project. Compound **4** has the gold (I) N-heterocyclic carbene moiety, but lacks ferrocene moieties. Compound **5** has the gold (I) N-heterocyclic carbene moiety, and two

ferrocene moieties per molecule. Compound **6** features a gold (I) N-heterocyclic moiety and four ferrocene moieties per molecule. Compound **7** is the ferrocenium of compound **5**, meaning that the iron in both ferrocenes per molecule is at a different oxidation state (3^+) than that of compound **5** (2^+). These compounds were featured in Arambula et al. 2016.

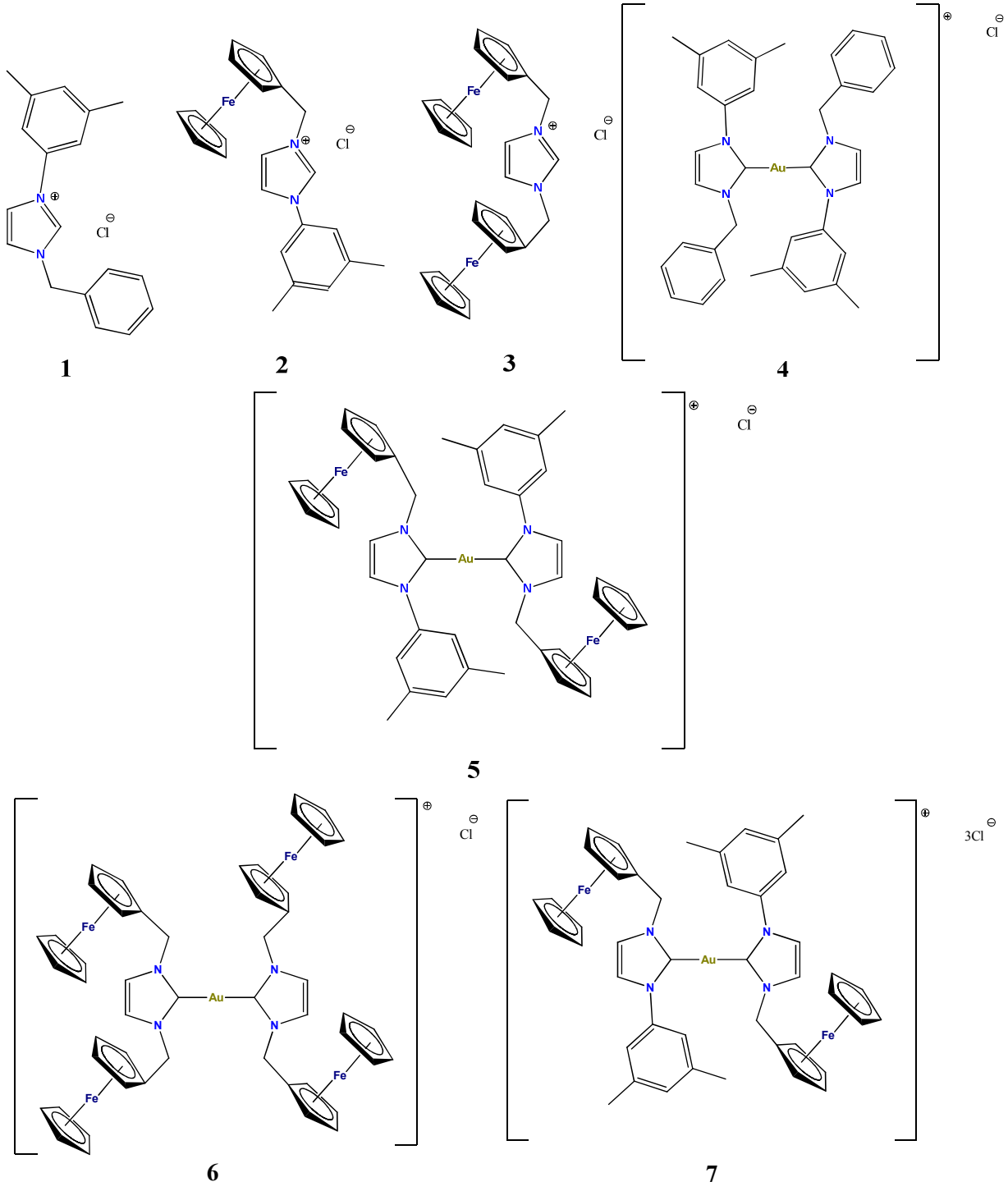

Figure 3. Structures of compounds 1-7.

Auranofin (Aura) is an FDA-approved anti-rheumatic drug that has been shown to inhibit thioredoxin reductase. It is a glucose analog with a gold (I) phosphine moiety.[8,9] Auranofin was used as a control for TrxR inhibition in the lipoate reduction assay, and its anti-proliferative potency was tested by the MTT assay for comparison purposes.

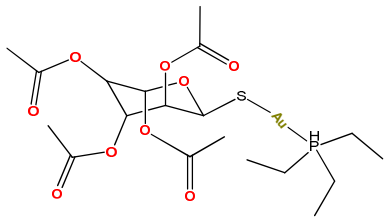

Auranofin

Figure 4. Structure of Auranofin.

Cell Proliferation as Determined by MTT Assay

The IC_{50} value of Auranofin in A549 was measured. This was done largely for comparison purposes, as slight protocol variations from one lab to the next make potency comparisons using data generated by another lab difficult. In the case of Auranofin, our average IC_{50} value was 1.14 +/- 0.15 µM. This allows us to make more accurate comparisons between our compounds and previously-established cytotoxic compounds, such as Auranofin.

The IC_{50} value of compound **6** in A549 was verified at Georgia Southern. Statistically, there was no discernable difference between values obtained at Georgia Southern by the author and values obtained in Texas by Dr. Arambula. Compound **6** has an average IC_{50} of 0.149 +/- 0.024 µM. Compound **6** is the most potent of these compounds, followed by compound **5** (0.39 +/- 0.01 µM), then compound **4** (0.71 +/- 0.03 µM). This trend shows increased toxicity of the experimental compounds as the number of ferrocene subunits per molecule is increased.

Table 1. Average IC_{50} values of compounds in A549 after three days incubation. Literature values provided for Cisplatin and Carboplatin for comparison.

Compound(s)	Average IC_{50} Value (μM)	Standard Error
2	6.4	1.1
3	13	1.5
4	0.71	0.03
5	0.39	0.01
6	0.14	0.03
1:2 4:3	0.61	0.05
Auranofin + 3	1.61	0.09
Auranofin	1.67	0.05
Cisplatin	0.98[a]	---
Carboplatin	27[a]	---

During previous work in Texas, compounds **5** and **7** were determined to yield indistinguishable results for the MTT assay. This was re-examined at Georgia Southern, to the same effect. There was no discernable difference between the A549 cells exposed to compound **5** and A549 cells exposed to the same concentrations of compound **7** (p=0.5066).

[a] Values from a currently unpublished work by Prof. Jonathan L. Sessler and Prof. Zahid Siddik. Cells were incubated with compound for 120 hr.

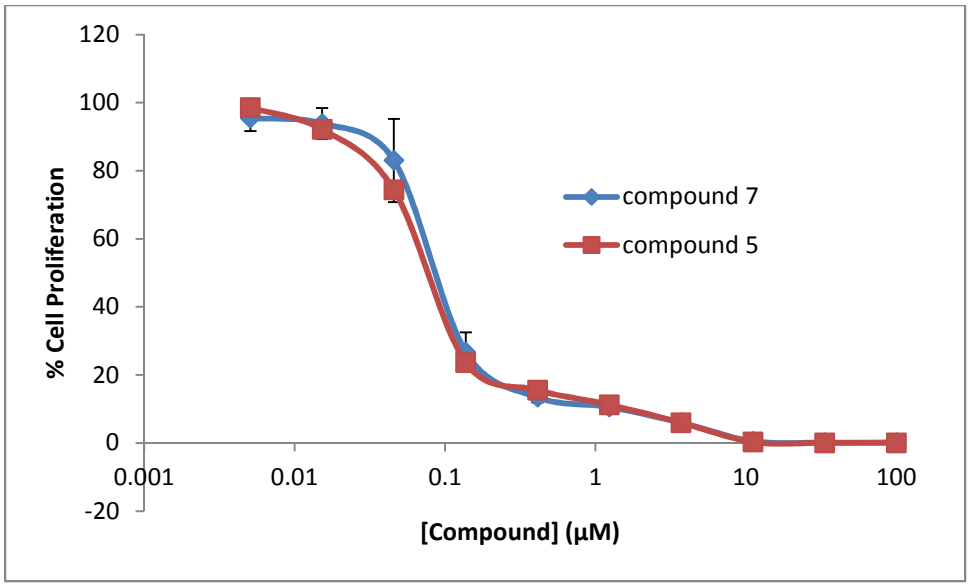

Figure 5. Average MTT data and standard error for compounds 5 and 7 in A549.

Determination of Intracellular ROS

In previous work by the Arambula group, it was shown that Auranofin and compound **4** generated about equal amounts of intracellular ROS after 6 hours incubation at 2.5 µM compound. It was also shown that the amount of intracellular ROS in A549 significantly increases with the addition of ferrocene subunits to the gold (I) N-heterocyclic core of the compounds. Compound **5** generates more intracellular ROS than compound **4**, but less than compound **6**. The intracellular ROS increase in A549 cells exposed to 2.5 µM of compounds **5** or **6** is significantly greater than that of cells exposed to 2.5 µM Auranofin at 6 hours of incubation.[31] This shows that compounds **4-6** are capable of increasing intracellular ROS levels.

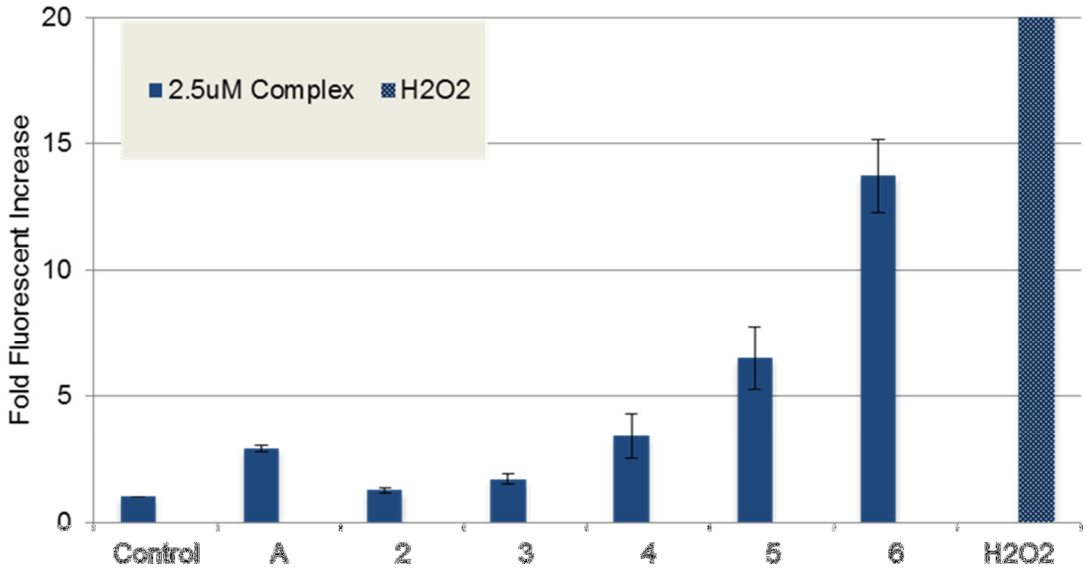

Figure 6. Relative intracellular ROS increase of A549 cells after 6 hours incubation with 2.5 µM compound. A is for Auranofin. Figure courtesy of Dr. Arambula.

Inhibition of Intracellular Thioredoxin Reductase by Lipoate Reduction Assay

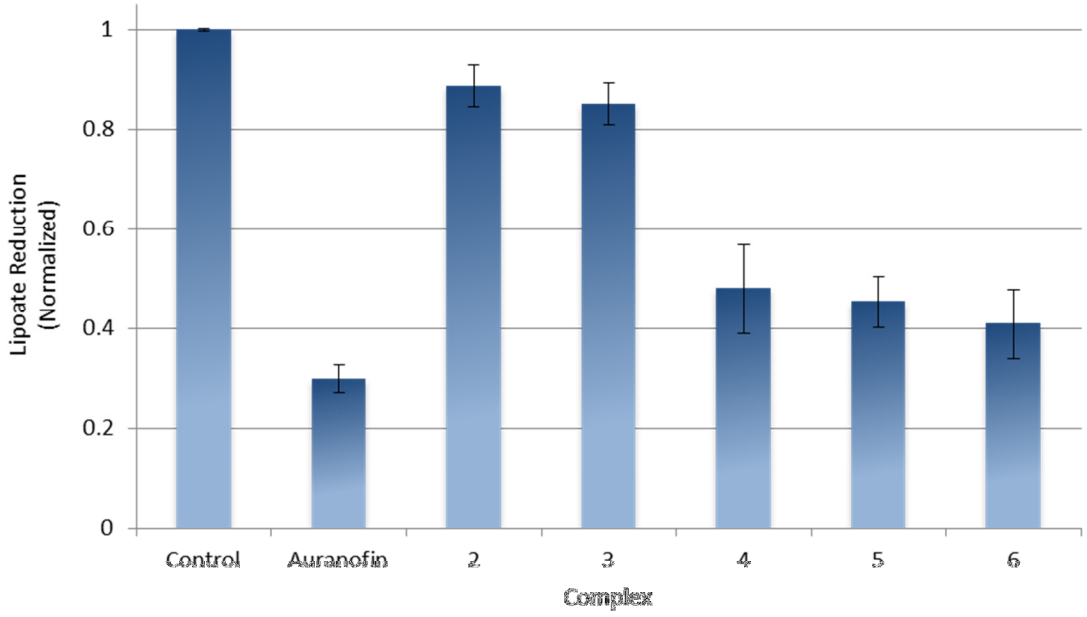

Figure 7. Normalized lipoate reduction and standard error in A549 at 2.5 µM compound, 180 minutes after addition of lipoate. Figure courtesy of Dr. Arambula.

As discussed in Arambula et al. 2016, Auranofin inhibits about 30% of intracellular TrxR activity. A549 cells incubated with compounds **2** and **3** did experience some inhibition of

thioredoxin reductase, but not a great deal. Cells exposed to compounds **4**, **5**, and **6** display about 50% inhibition of intracellular thioredoxin reductase. This shows that compounds **2-6** do inhibit the antioxidant enzyme thioredoxin reductase.[31]

Conclusions from Previous Work

The work published in Arambula et al. 2016 showed that compounds **4**, **5**, and **6** were all highly toxic to A549 lung cancer cells. They all induced elevated levels of intracellular ROS and inhibited the activity of intracellular TrxR. These compounds successfully targeted multiple points along the antioxidant pathway, leading to their high potency.[31]

Chapter 2. Small Molecule Design Parameters and Approach

2.1 Introduction of Compounds 8-11

To test our hypothesis of multi-modal pathway targeting, a small library of complexes were designed and synthesized in collaboration with Professor Kuppuswamy Arumugam at Wright State University. For these studies, quinone-based moieties (via naphthoquinone) were chosen due to their biological relevance. Lead compound **9** consists of two naphthoquinone moieties appended to an N-heterocyclic carbene (NHC). It is proposed that the dual combination of 1) a redox cycling agent to increase exogenous ROS and 2) a Au(I)-NHC to inhibit a reducing metabolite (i.e. TrxR) to lower the upper threshold of the functional range will disrupt antioxidant homeostasis from both ends, thus overwhelming the network and promoting cell death (Figure 8). Naphthoquinone precursor **8** in addition to mono-NHCs **10** and **11** provide both charged (non-metal coordinated) and neutral metal coordinated controls. These compounds will help develop a Structure Activity Relationship to elucidate parameters important in the design of metal coordinated NHC medicinal agents.

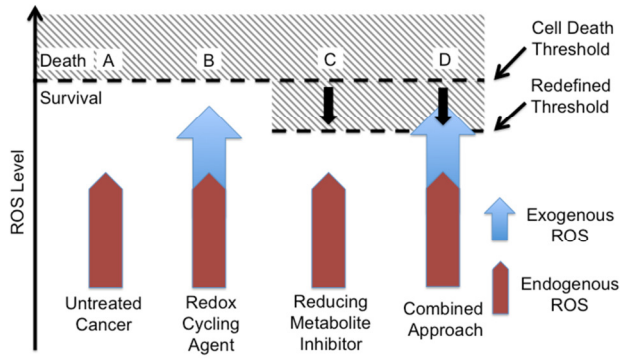

Figure 8. Mechanism-based rationale regarding a dual-targeting approach in drug design. A) Untreated cancer cells elicit a defined and tolerated endogenous ROS level. This level is below the threshold that induces cell death. B) Many small molecules are capable of accentuating exogenous ROS within the cancer, but may not reach the threshold, or require higher levels of redox cycler to overwhelm the system. C) Antioxidant inhibitors reduce the amount of reducing metabolite, thus lowering the upper threshold. D) The dual targeting approach proposes the use of a redox cycler to accentuate exogenous ROS in combination with a reducing metabolite inhibitor, which lowers the threshold. This combination will overwhelm the system and drive it towards death.

Doxorubicin (Dox) is an FDA-approved anticancer therapeutic, which is currently in use. It is structurally similar to the second generation of our compounds in that it has a naphthoquinone moiety.[32] Doxorubicin was also studied by MTT assay, lipoate reduction assay, thermal denaturation, and flow cytometry for intracellular ROS and apoptosis detection.

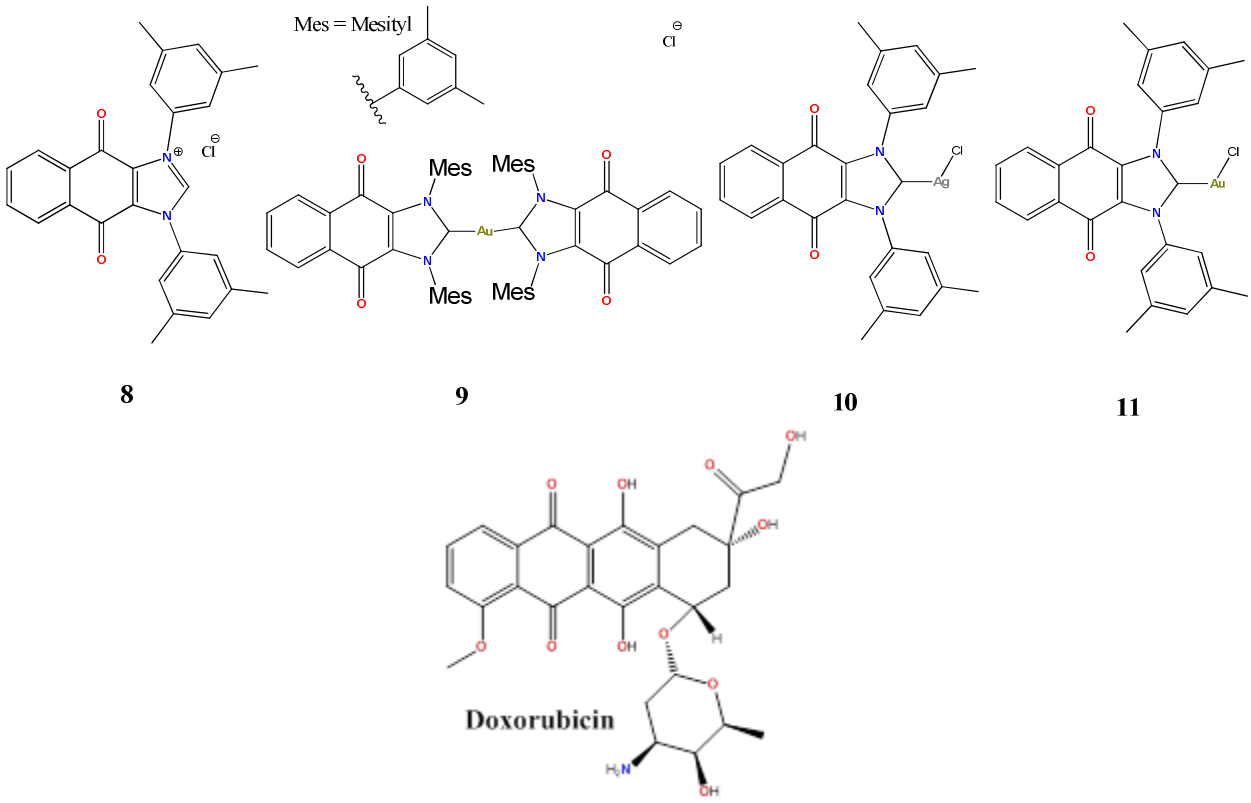

8 **9** **10** **11**

Figure 9. Structures of compounds 8-11 and Doxorubicin.

2.2 Utility of Quinone-based Moieties in Targeting the Antioxidant Pathway

While the first generation of compounds utilized ferrocene moieties for redox cycling, the second generation compounds utilized quinones for redox cycling. Quinones are known to be redox-active in the cell, as they are involved in the electron transport chain in mitochondria, and in photosynthesis. Quinones can cycle two electrons per moiety (from quinone to semiquinone to hydroquinone and back),[4] while ferrocenes can only cycle one electron per moiety (from ferrocene to ferrocenium and back). Quinone incorporation within our design is proposed to increase intracellular exogenous ROS.

2.3 Utility of Au(I) NHCs in Targeting the Antioxidant Pathway

The gold (I) bis-N-heterocyclic carbene moiety has been shown to be effective in inhibition of intracellular TrxR.[8,9] Inhibition of the antioxidant enzyme thioredoxin reductase should indirectly lead to an increase in intracellular ROS, which should lead to cell death. Compound **4** from the first generation of compounds is intended to show the effect of just the gold (I) bis-N-

heterocyclic carbene moiety. Compound **9** incorporates both the naphthoquinone and gold (I) bis-N-heterocyclic carbene.

2.4 Mono vs. Bis/ Gold vs. Silver

Comparison of compounds **9** and **11** is intended to be beneficial in revealing the role of the second N-heterocyclic carbene moiety in the experimental small molecules. Compound **11** is a naphthoquinone with a gold (I) mono-N-heterocyclic carbene moiety. Compound **10** is intended to show the difference in efficacy between gold and silver as the transition metal complexed with the N-heterocyclic carbene when compared with compound **11**.

2.5 Assays and Tests Introduced for Study of 8-11

A few new assays and tests were introduced for work involving the new compounds. These include the FITC Annexin V Apoptosis Assay, determination of DNA binding by thermal denaturation, the zebrafish toxicity screening, and the *in vivo* studies of compounds 6 and 9 in xenografts.

An FITC Annexin V Apoptosis Detection Kit was used to determine whether treated cells were undergoing apoptosis or necrosis. Annexin V is a protein that binds the phospholipid phosphatidylserine. During apoptosis, phosphatidylserine that was on the inner membrane of the cell shifts to the outer membrane of the cell. This allows interaction of extracellular Annexin V with shifted phosphatidylserine. The FITC-Annexin V kit that we used utilizes this by affixing a fluorophore to the Annexin V, such that when Annexin V binds exposed phosphatidylserine, the FITC fluoresces. By simultaneously treating cell populations with propidium iodide (which only penetrates dead cells through the gaps in their membranes) and FITC-Annexin V, cells with high red fluorescence due to propidium iodide penetration can be excluded from the population of interest. Under these conditions, live, thriving cells will not fluoresce red (with propidium iodide) or green (with FITC-Annexin V). Also under these conditions, cells in early apoptosis will fluoresce green, but not red. Any cells under these conditions that fluoresce red are either dead or very nearly there, and the pathway by which they got there cannot be determined unless they were previously monitored in a time-dependent fashion (do the cells go from no fluorescence, to green fluorescence, then both green and red, or do they go directly from no

fluorescence to red fluorescence?). Cells that go directly from no fluorescence to red fluorescence after constant monitoring are understood to undergo necrosis.[33]

Chapter 3. Results

3.1 Cell Proliferation by MTT Assay

In May of 2015, compounds **8** and **9** were first introduced to the cells. Compound **8** is the 2nd generation's equivalent of compound **3** from the 1st generation of compounds.[31] As such, it displayed a lower potency in inhibiting cell proliferation than compound **9**. The IC_{50} value of **8** was 1.31 +/- 0.22 µM in A549. This was significantly different from compound **9**'s IC_{50} of 0.076 +/- 0.013 µM in A549 ($p < 0.0001$). The high potency of compound **9** further supported the hypotheses behind the design of the compound, and resulted in compound **9** joining compound **6** on the short list of lead compounds for potential drug development.

As discussed in Arambula et al. 2016, it is important to know if the increased activity of lead compound **9** is due only to the presence of all moieties in a given proportion, or if there is some advantage to having all of the moieties on a single molecule. This is why cocktails of Auranofin + **3** and **3+4** were studied during development of lead compound **6.**[31] The cocktail used for this purpose for compound **9** was a 1:2 molar ratio of **4:8**. Compound **4** was the gold (I) N-heterocyclic carbene in this mixture, and compound **8** was the naphthoquinone. The average IC_{50} value of 1:2 **4:8** in A549 was 0.197 +/- 0.057 µM, which was a statistically different value from that of compound **9** in A549 (0.076 +/- 0.013 µM, p=0.0484). The cocktail was more potent than compound **4** alone in A549 (0.59 +/- 0.12 µM, p=0.009) and compound **8** alone in A549 (1.31 +/- 0.22 µM, p=0.0011). The potency of the cocktail was indistinguishable from that of Doxorubicin (0.103 +/- 0.024 µM, p=0.566) or compound **6** (0.149 +/- 0.024 µM, p=0.7059).

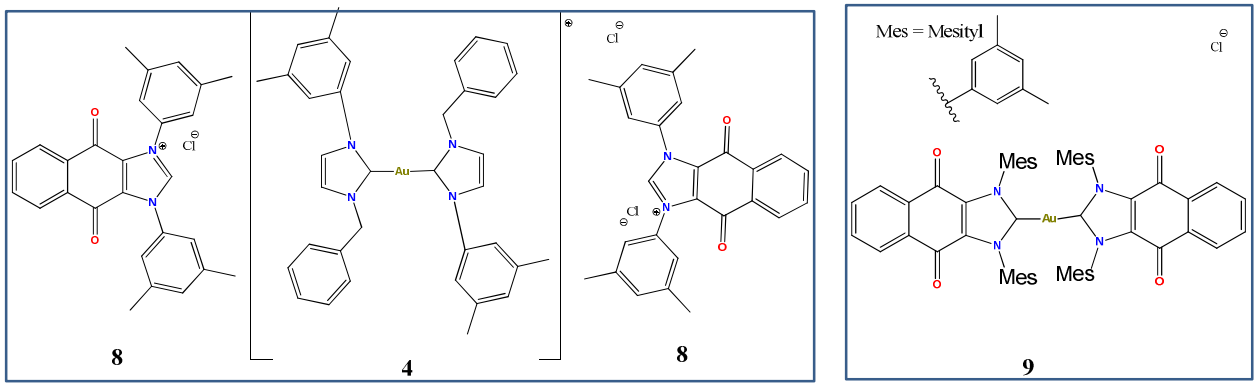

Figure 10. Structures of 1:2 4:8 cocktail and compound 9.

In A2780, the average IC_{50} value for compound **8** was 0.159 +/- 0.052 µM, which is not significantly different from that of compound **9** at 0.041 +/- 0.013 µM (p=0.0748). This is probably because the A2780 is difficult to work with, as it is very sensitive and cells of this line die easily. This caused some erratic responses from the cell line. Given time, more work could be done with these compounds in this cell line, and the error could be cleaned up a bit, which may make a difference in compound potency more evident. In A2780CP, the average IC_{50} value of compound **9** was 0.054 +/- 0.006 µM. This was significantly different from that of compound **8**, which was 0.703 +/- 0.119 µM (p=0.0064). In PC-3, there was no discernable difference between the potency of compound **8** (0.136 +/- 0.020 µM) and compound **9** (0.104 +/- 0.015 µM, p=0.2513).

Compound **10** was first introduced to the A549 cell line in April of 2016. The IC_{50} value of compound **10** in A549 was determined to be 0.61+/- 0.04 µM. This potency is distinct from all other compounds studied except compound **4** (p=0.8545). Compound **11** has an average IC_{50} value of 12.06 +/- 0.18 µM in A549. This value is statistically different from that of all other compounds tested (p<0.0001). The compounds displayed varying levels of toxicity, with compounds 6 and 9 being the most potent, due to their redox capabilities and gold(I) NHC centers.

Table 2. IC_{50} values of compounds in A549.

Compound(s)	Average IC_{50} (µM)	Standard Error
4	0.59	0.12
6	0.149	0.024
8	1.31	0.22
9	0.076	0.013
10	0.61	0.04
11	12.06	0.18
Auranofin	1.14	0.15
Doxorubicin	0.103	0.024
1:2 4:8	0.197	0.057

Table 3. P-values of t-tests comparing IC_{50} values of compounds in A549. Values less than 0.05 are significant.

	Dox	8	9	Aura	1:2 4:8	4	6	10
Dox	---	<0.0001	0.0753	<0.0001	0.566	0.0005	0.8114	<0.0001
8	<0.0001	---	<0.0001	0.9686	0.0011	0.0693	0.0008	0.0474
9	0.0753	<0.0001	---	<0.0001	0.0484	<0.0001	0.0117	<0.0001
Aura	<0.0001	0.9686	<0.0001	---	0.0006	0.0479	0.0005	0.0281
1:2 4:8	0.566	0.0011	0.0484	0.0006	---	0.009	0.7059	0.0001
4	0.0005	0.0693	<0.0001	0.0479	0.009	---	0.0041	0.8545
6	0.8114	0.0008	0.0117	0.0005	0.7059	0.0041	---	<0.0001
10	<0.0001	0.0474	<0.0001	0.0281	0.0001	0.8545	<0.0001	---
11	<0.0001	<0.0001	<0.0001	<0.0001	<0.0001	<0.0001	<0.0001	<0.0001

Table 4. Average IC_{50} values and standard error of compounds in A2780, A2780CP, and PC-3.

Cell Line	Compound	Average IC_{50} (μM)	Standard Error
A2780	6	0.194	0.002
	8	0.159	0.052
	9	0.041	0.013
A2780CP	6	0.120	0.003
	8	0.703	0.119
	9	0.054	0.006
PC-3	6	0.475	0.079
	8	0.136	0.020
	9	0.104	0.015

Table 5. P-values of t-tests comparing IC_{50} values of compounds in A2780, A2780CP, and PC-3. Values less than 0.05 are significant.

	Cell Line	A2780			A2780CP			PC-3		
Cell Line	Compound	6	8	9	6	8	9	6	8	9
A2780	6	---	0.8799	<0.0001	<0.0001	0.0068	<0.0001	0.0119	0.0457	0.0014
	8	0.8799	---	0.0748	0.4326	0.0209	0.1543	0.0481	0.4178	0.2142
	9	<0.0001	0.0748	---	0.0055	0.0018	0.4732	0.0016	0.0079	0.0214
A2780CP	6	<0.0001	0.4326	0.0055	---	0.0103	0.0008	0.0126	0.5983	0.4768
	8	0.0068	0.0209	0.0018	0.0103	---	0.0064	0.1757	0.0006	0.0010
	9	<0.0001	0.1543	0.4732	0.0008	0.0064	---	0.0064	0.0267	0.0568
PC-3	6	0.0119	0.0481	0.0016	0.0126	0.1757	0.0064	---	0.0010	0.0013
	8	0.0457	0.4178	0.0079	0.5983	0.0006	0.0267	0.0010	---	0.2513
	9	0.0014	0.2142	0.0214	0.4768	0.0010	0.0568	0.0013	0.2513	---

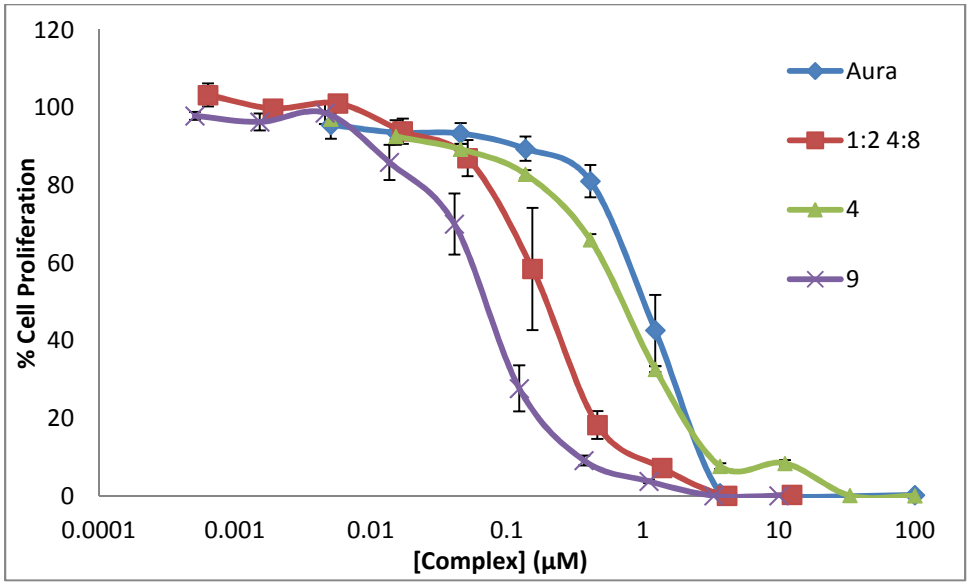

Figure 11. Average MTT data and standard error for Auranofin, 1:2 4:8 cocktail, 4, and 9 in A549.

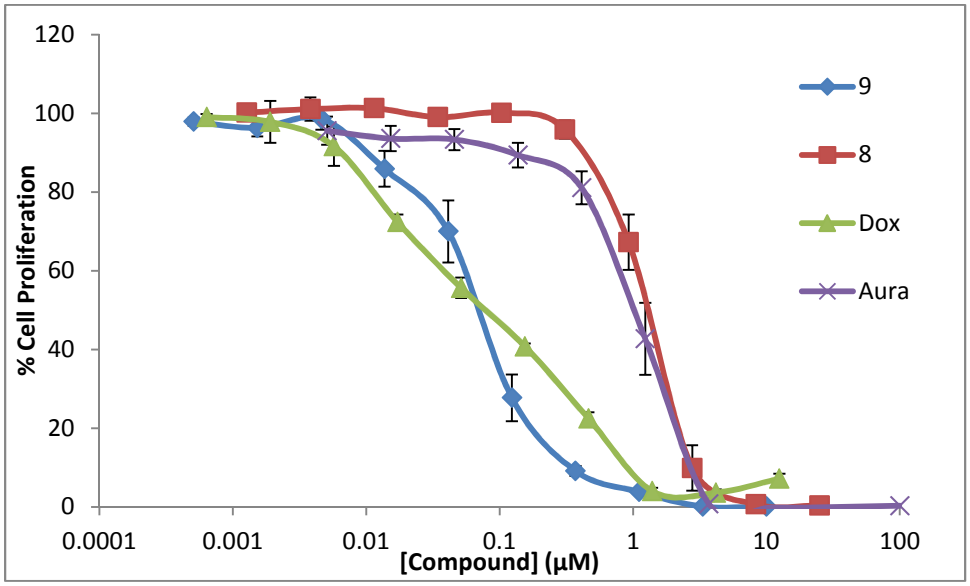

Figure 12. Average MTT data and standard error for compounds 8, 9, Doxorubicin, and Auranofin.

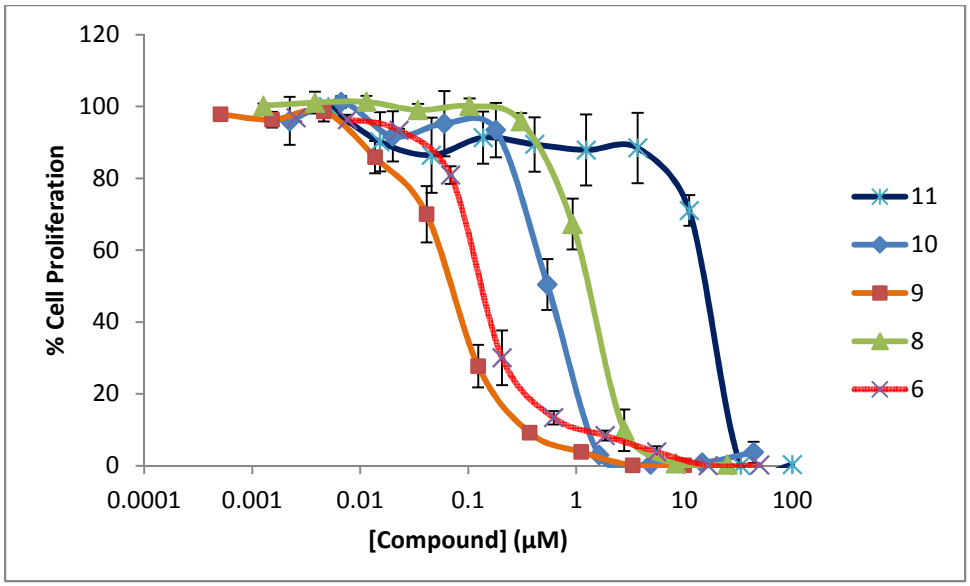

Figure 13. Average MTT data and standard error for compounds 6, 8, 9, 10, and 11.

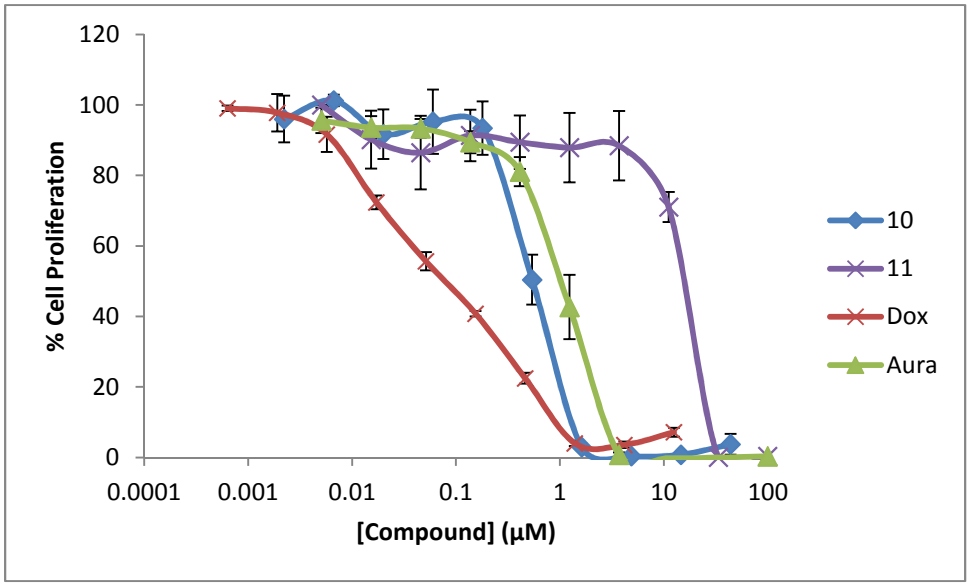

Figure 14. Average MTT data and standard error for compounds 10, 11, Doxorubicin, and Auranofin.

3.2 Cellular Uptake as Determined by Lowry Assay and ICP-MS

After some fine-tuning of the protocol (how much of which acids to use for digestion, how and when to quantify the cells in each sample, etc.), we arrived at the protocol described in Materials and Methods. This protocol allows for normalization of the data obtained from the Inductively-Coupled Plasma Mass Spectrometer (ICP-MS) by the Modified Lowry Assay.

Samples were generally found to contain about 20,000 µg/mL protein. According to the normalized ICP-MS data, as shown in Figure 15, about 4 times more gold is getting into the cells treated with Auranofin than cells treated with either of compounds **4** or **9**. While this is slightly disappointing from an uptake perspective, it may indicate that compounds **4** and **9** are more potent per molecule than Auranofin. The IC_{50} value of Auranofin is about twice that of compound **4**, and 15 times that of compound **9**. Keeping in mind that a lower IC_{50} value denotes higher anti-proliferative potency, this could mean that our compounds are far more potent per molecule than Auranofin.

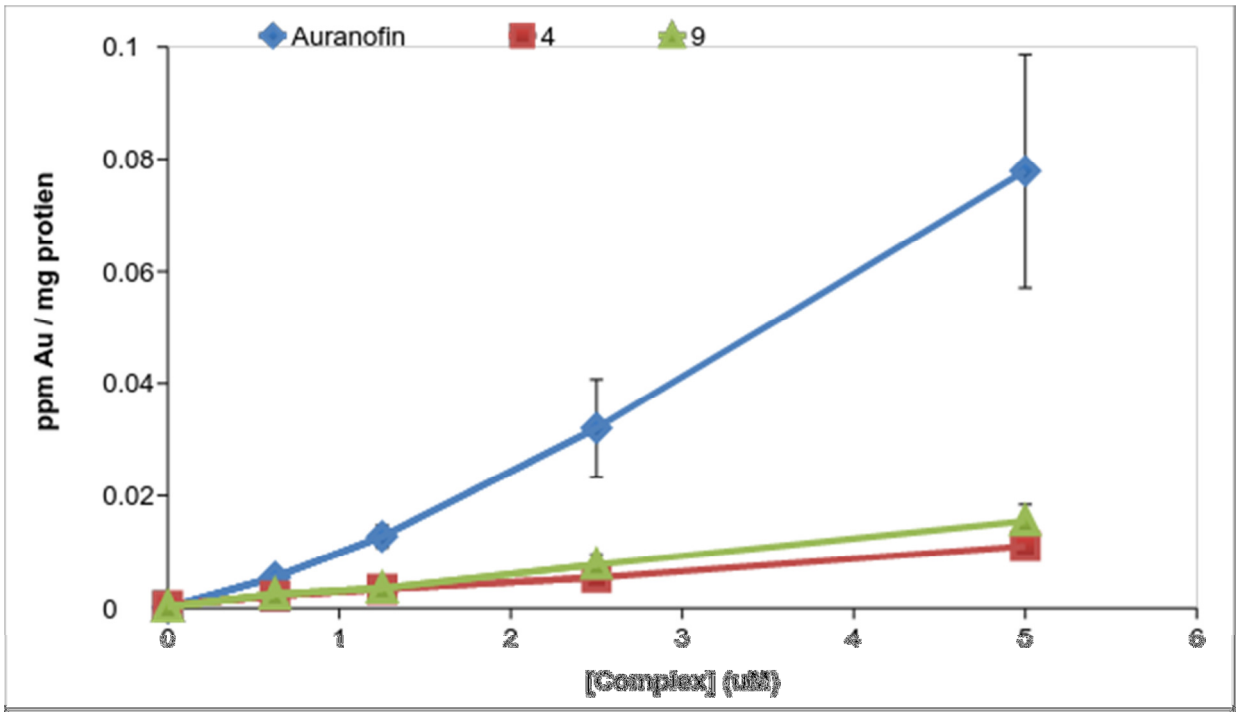

Figure 15. Average intracellular gold (normalized to protein) after exposure of A549 to varying concentrations of Auranofin, 4, and 9, with standard error. Figure courtesy of Dr. Arambula.

3.3 Serum Protein Binding Study

An important piece of information to know in the development of potential therapeutics is the amount of free drug in blood serum after drug administration. In an effort to determine the amount of free drug in blood serum after administration, the concentration of gold not bound to serum proteins over the course of time was monitored by ICP-MS. Fetal bovine serum that has not been heat-inactivated is commonly used for this purpose.[34] There is a possibility that the drug

subunits disassociate in serum such that measuring free gold is not equivalent to measuring free drug. For this reason, the distinction between free gold and free drug must be made at this time. Future experimentation utilizing LC-MS for detection of organic subunits is of great interest to the group, but has not yet been scheduled. As shown in Figure 16, the gold in Auranofin binds serum proteins within 6 hours, while the gold in compounds **4** and **9** remains free even after 72 hours.

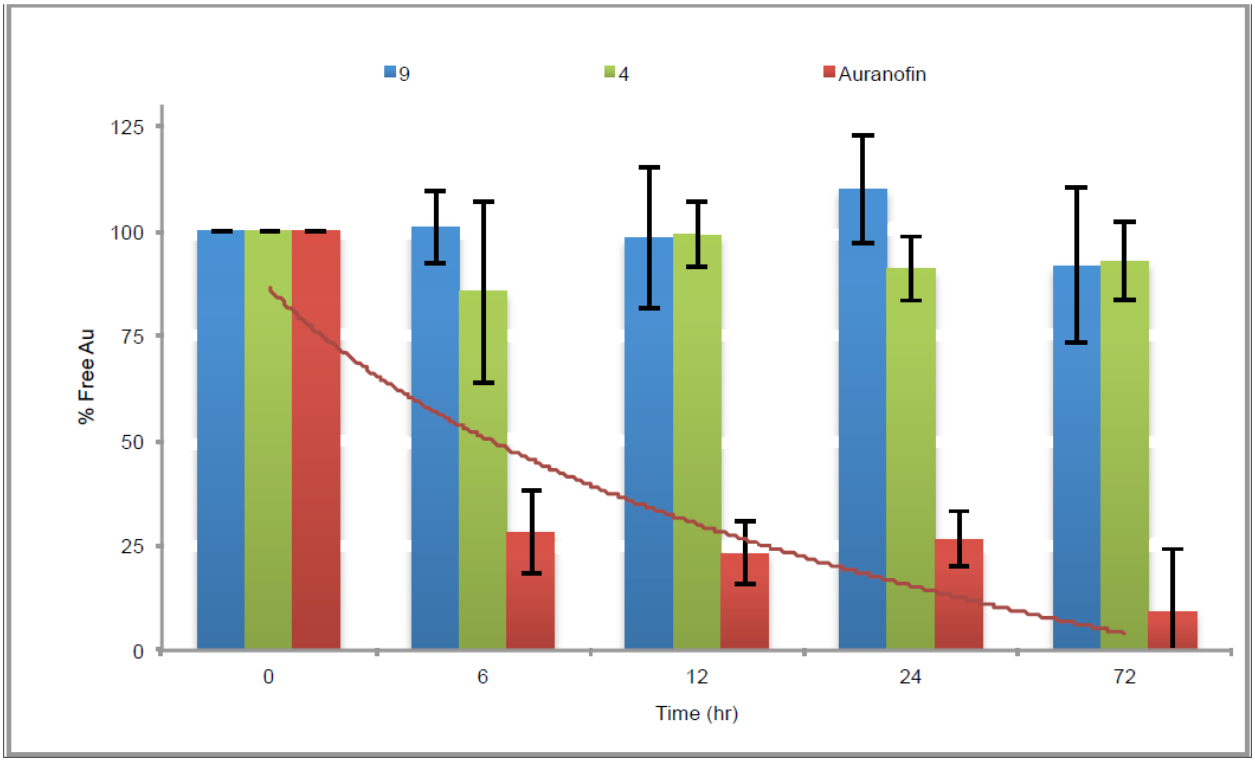

Figure 16. Average percent free gold at varying time points after introduction of Auranofin, 4, and 9 to fetal bovine serum at 37°C, with standard error. Graph courtesy of Dr. Arambula.

3.4 Determination of Intracellular ROS

In 2016, the Arambula group had the opportunity to use the flow cytometer at UT Austin, so intracellular ROS data for compounds **8** and **9**, the 1:2 **4:8** cocktail, and Doxorubicin. Figure 17 shows the dose-responsive nature of the intracellular ROS increase after 6 hours incubation with compound **9**.

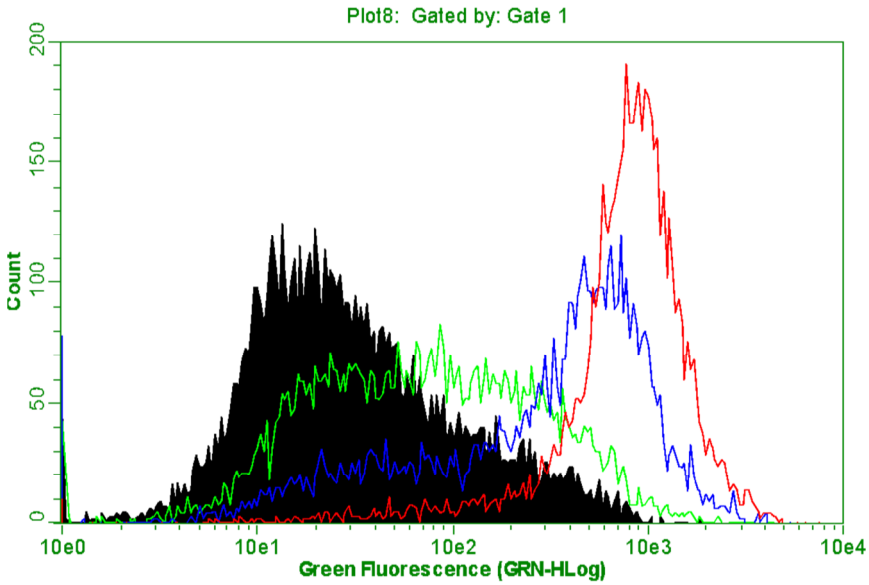

Figure 17. Overlaid flow cytometry data for ROS levels in A549 cells incubated with varying concentrations of compound 9 for 24 hours. The population depicted in black is the vehicle control, the green population is 1.25 µM 9, the population in blue is 2.5 µM 9, and the population in red is 5 µM 9. Figure courtesy of Dr. Arambula.

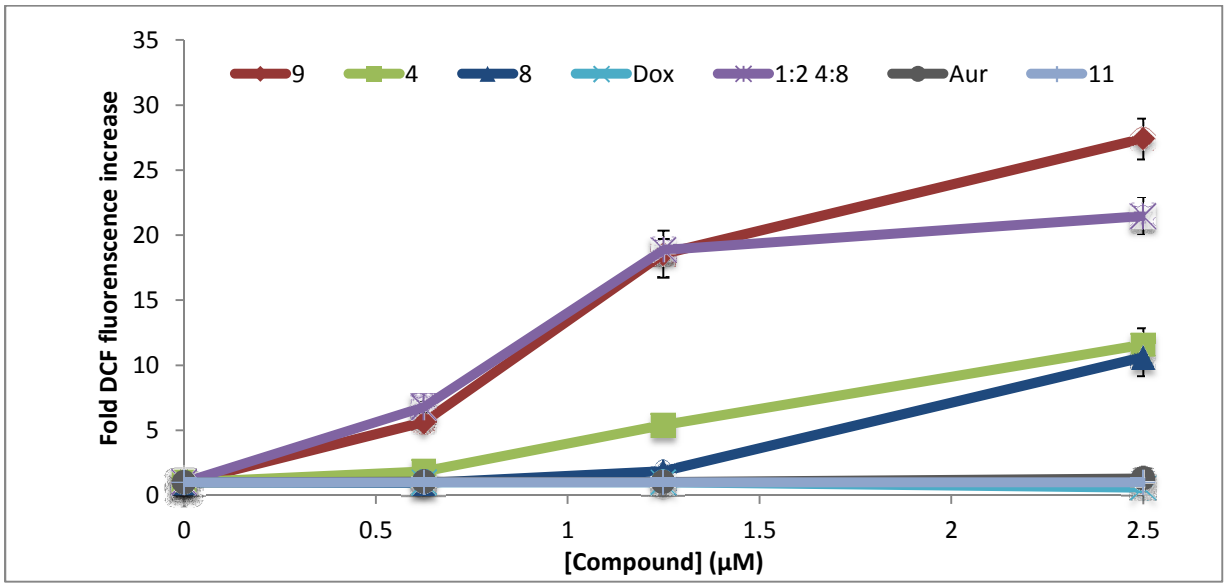

Figure 18. Relative intracellular ROS levels of A549 after 6 hours incubation with varying concentrations of compound. Figure courtesy of Dr. Arambula.

As can be seen in Figure 18, compound **9** and the 1:2 **4:8** cocktail increased intracellular ROS levels the most, with at least a 20-fold increase at 2.5 µM compound. The difference between this increase and the increase caused by compound **8** alone and compound **4** alone lead us to

believe that the effect of having both the quinone and the N-heterocyclic carbene present on the molecule is at least additive, if not synergistic. At 2.5 µM, both compounds **4** and **8** displayed about a 10-fold increase in intracellular ROS. Surprisingly, mono-NHC **11** provided no detectable accentuation of intracellular ROS under the assay conditions. While its mechanism has yet to be fully elucidated, it is possible that the more reactive Au-Cl bond within **11** may be a site of protein sequestration. Alternatively, the neutrality within **11** (relative to the single positive charge within **9**, **4**, **8**) may prevent or create an alternative route of cellular uptake, thus leading to its reduced activity.[35] Despite this, lead compound **9** and charged controls (i.e. **4**, **8**) were able to generate intracellular ROS, fulfilling one half of the proposed mechanism of action. It can be noted that while Auranofin is known to inhibit TrxR,[8,9] there is not much of an intracellular ROS increase in cells treated with Auranofin relative to cells treated with our experimental compounds. This leads us to believe that the redox cycling of the naphthoquinones is largely responsible for the increase.

3.5 Inhibition of Intracellular Thioredoxin Reductase by Lipoate Reduction Assay

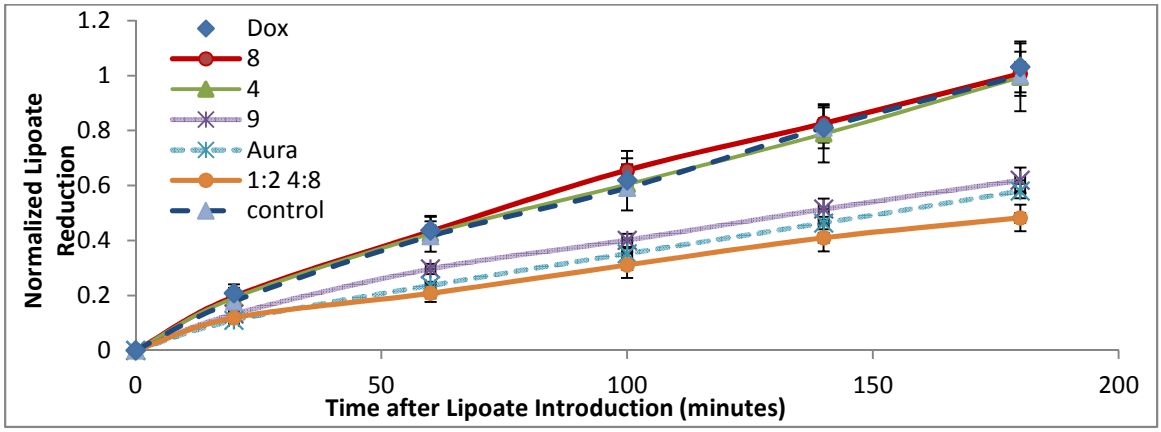

Figure 19. Normalized lipoate reduction with standard error in A549 over 3 hours, after 6 hours incubation in 0.625 µM compound.

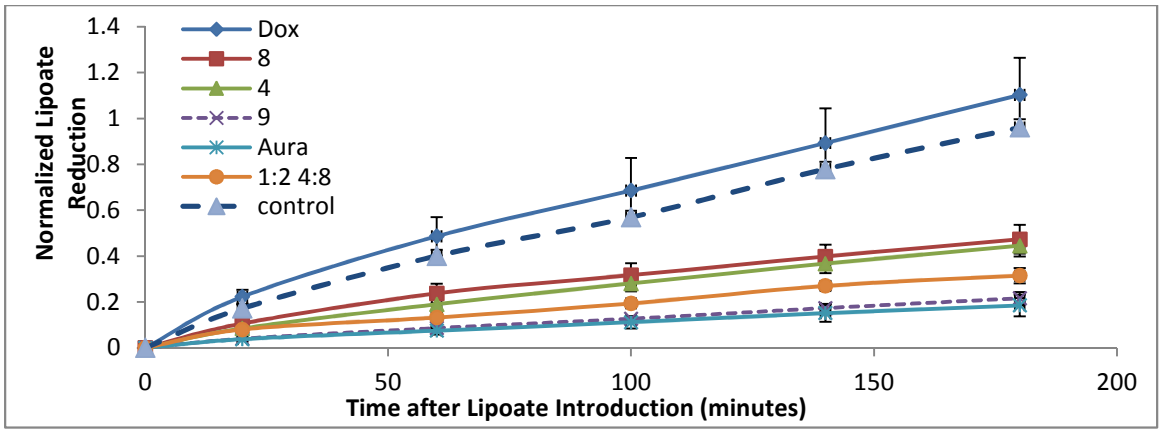

Figure 20. Normalized lipoate reduction with standard error in A549 over 3 hours, after 6 hours incubation in 5 µM compound.

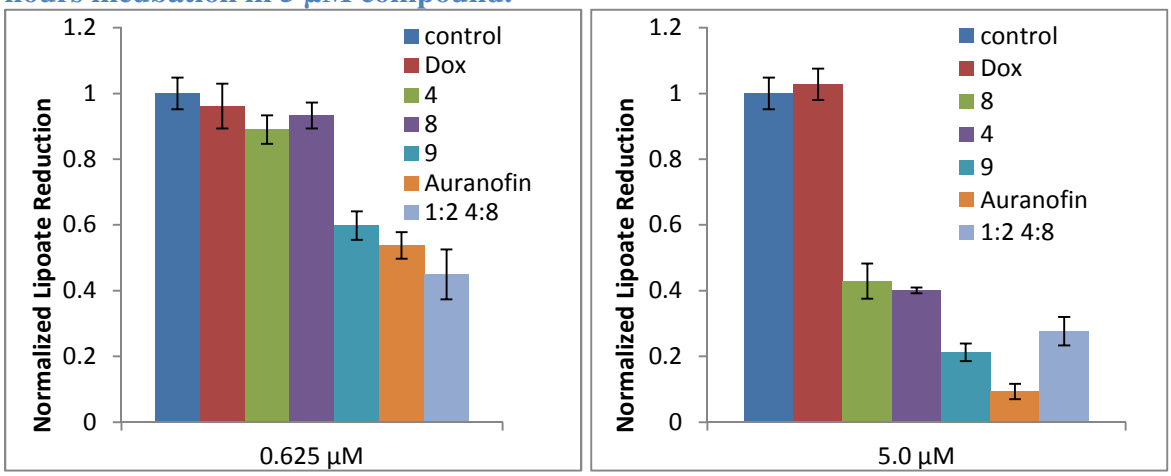

Figure 21. Normalized lipoate reduction and standard error in A549 at 5 µM and 0.625 µM compound, 180 minutes after addition of lipoate.

Because Auranofin is known to inhibit TrxR activity, it was used as a positive control for TrxR inhibition. Auranofin inhibited TrxR activity significantly at all concentrations studied ($p \leq 0.0001$). This can be seen in Figures 20-25, 34-39, 46, and 47, and Table 12. Auranofin inhibited thioredoxin reductase activity from 29 +/- 6 % inhibition at 0.156 µM to 91 +/- 2 % inhibition at 5 µM. Doxorubicin was used for the purpose of comparing the activity of our naphthoquinone compounds against a structurally-similar FDA approved anticancer drug. Although Doxorubicin has been shown to inhibit TrxR in human rhabdomyosarcoma cells, we found that it does not inhibit TrxR in A549 within 9 hours of being introduced to the cells.[13] Statistically, there was no difference between the untreated cells and cells treated with 5 µM Doxorubicin, or any lower concentrations ($p=0.0898$ - 0.5855).

Of the other compounds run, compound **9** and the 1:2 **4:8** cocktail showed significant TrxR inhibition at all concentrations studied ($p \leq 0.0012$ and $p \leq 0.0182$, respectively). Compound **9**

activity ranged from about 33 +/- 2 % inhibition of TrxR at 0.156 µM to 79 +/- 2 % inhibition at 5 µM. The 1:2 **4:8** cocktail displayed 18 +/- 3 % inhibition of thioredoxin reductase at 0.156 µM to 72 +/- 4 % inhibition at 5 µM. With the exception of the response seen at 0.3125 µM **4** ($p=0.1276$), compound **4** alone significantly inhibited TrxR at all studied concentrations ($p\leq0.0481$). Compound **4** alone inhibited TrxR from 11 +/- 3 % inhibition at 0.156 µM to 60 +/- 1 % inhibition at 5 µM. No significant inhibition was seen at 0.3125 µM **4**. Compound **8** was indistinguishable from the control at concentrations of 1.25 µM and below ($p\geq0.1170$). However, at 2.5 µM and 5 µM, compound **8** showed extremely significant inhibition of thioredoxin reductase ($p<0.0001$). At 2.5 µM, compound **8** inhibited 33 +/- 4 % TrxR activity, and at 5 µM, it inhibited 57 +/- 5 % TrxR activity. Compound **10** showed significant inhibition of TrxR at 1.25 µM and above ($p<0.0001$). At these concentrations, compound **10** is indistinguishable from Auranofin with regard to enzyme inhibition. Compound **11** did not significantly inhibit TrxR at any concentration below 5 µM. All of the compounds studied, including Auranofin and Doxorubicin, had a generally linear, dose-responsive effect on TrxR activity (although the slope of that line is about 0 for Doxorubicin). This is shown in Figures 40-45. Compounds **8-10** and the 1:2 **4:8** cocktail showed significant inhibition of thioredoxin reductase at 5 µM, demonstrating a second mechanism of action (with intracellular ROS increase being the first).

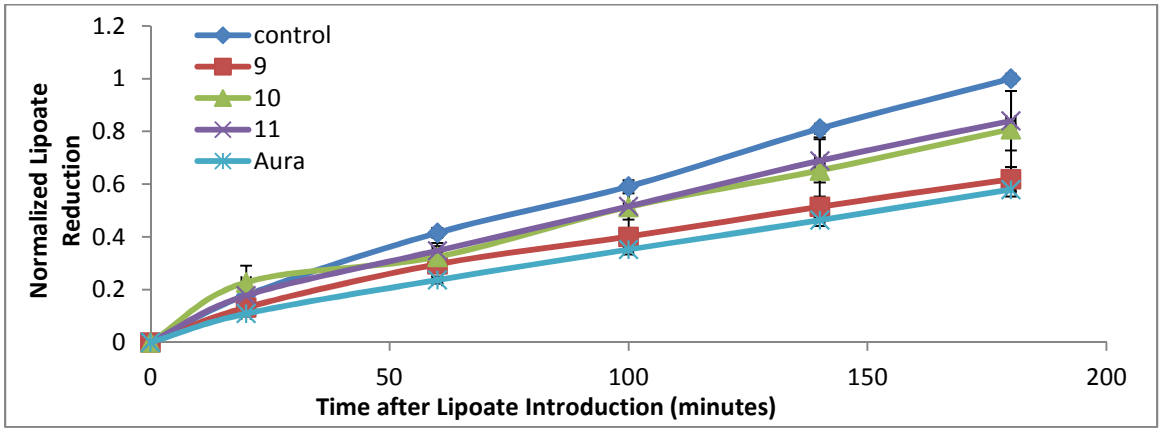

Figure 22 . Normalized lipoate reduction with standard error in A549 over 3 hours, after 6 hours incubation in 0.625 µM compound.

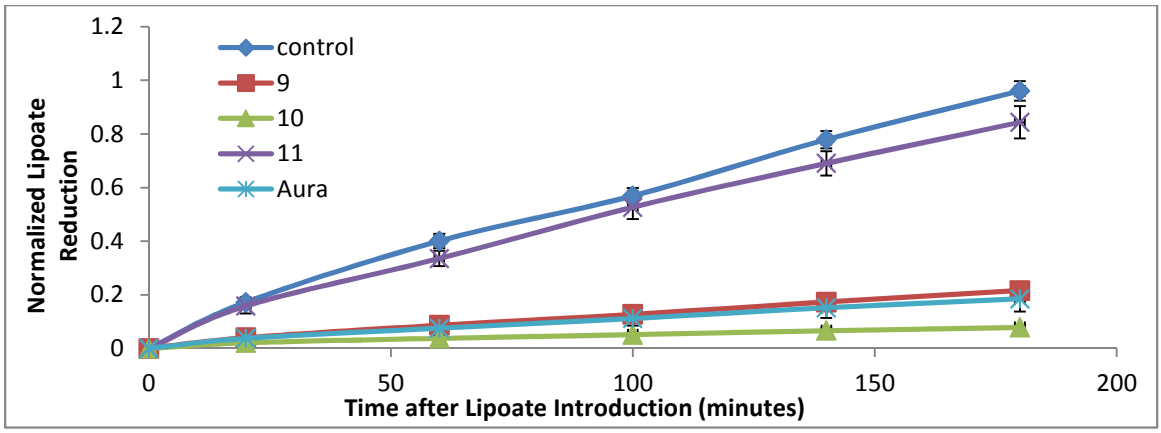

Figure 23. Normalized lipoate reduction with standard error in A549 over 3 hours, after 6 hours incubation in 5 µM compound.

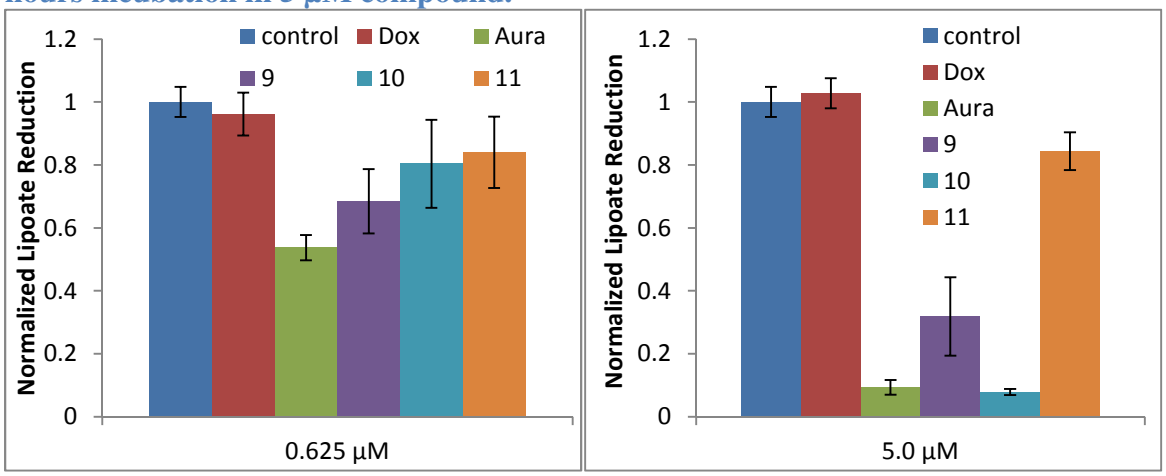

Figure 24. Normalized lipoate reduction with standard error in A549 at 0.625 µM and 5 µM compound, 180 minutes after addition of lipoate.

3.6 Determination of Cell Death Pathway by FITC Annexin V

Differentiation in cell death mechanisms is imperative to a full understanding in drug mechanistic action. Chaotic cell death such as necrosis is often viewed as problematic due to its lack of control and premature release of active biomolecules.[36] Apoptosis, on the other hand, is controllable and normal. Some anomalies, such as webbed feet and toes, are actually due to failure of the involved cells to undergo apoptosis.[37] It has been well established that Doxorubicin and Au(I) based complexes such as Auranofin induce controlled cell death via apoptosis in a variety of human cell lines.[32,38–40] In addition, quinone complexes, despite their inhibitory mechanism, also have been shown to induce apoptosis.[40] To further elucidate the mechanism of action regarding **9** in the A549 lung cancer model, flow cytometry was utilized to deduce the induction of apoptosis via fluorescent staining with Annexin-V. In brief, plated exponential

growth phase A549 cells were exposed to various concentrations of **9** and incubated for 24 hr. At that point, all cells (adhered and floating) were collected, washed, and stained with fluorescein labeled Annexin-V and propidium iodide (PI) and subjected to flow cytometry for the detection of both early stage apoptosis and late stage apoptosis/necrosis (cf. Figure 25). In a dose-responsive manner, the detection of early-stage apoptosis, as assessed by Annexin-V binding phosphatidylserine on the still intact and impermeable cell membrane (resulting in only FITC fluorescence), became evident. The treatment of A549 cells with Doxorubicin (a known inducer of apoptosis) provided similar results in both early and late stage apoptotic quadrants thus suggesting that complex **9** induces controlled cell death via an apoptotic mediated mechanism.

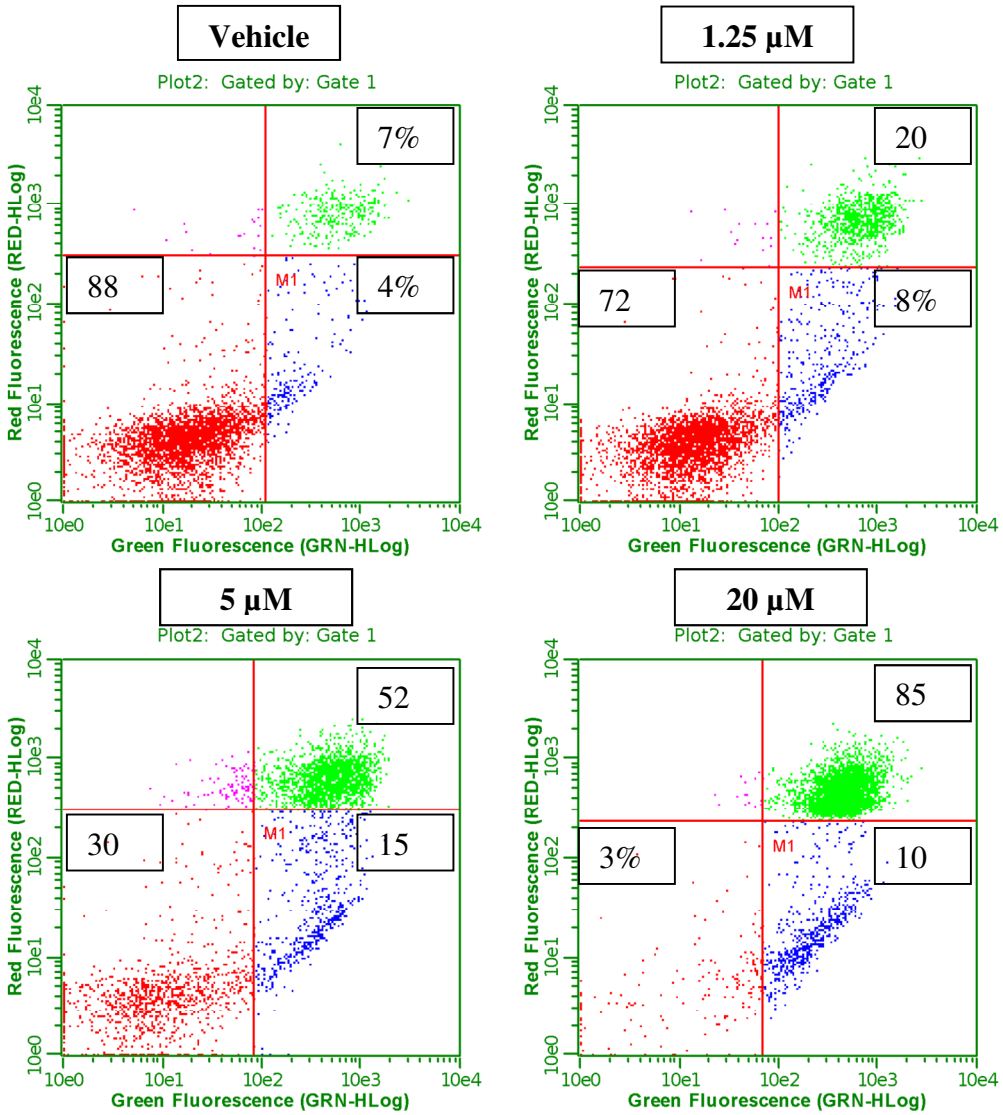

Figure 25. Representative Annexin V flow cytometry data for varying concentrations of compound 9 at 24 hours of incubation. Figure courtesy of Dr. Arambula.

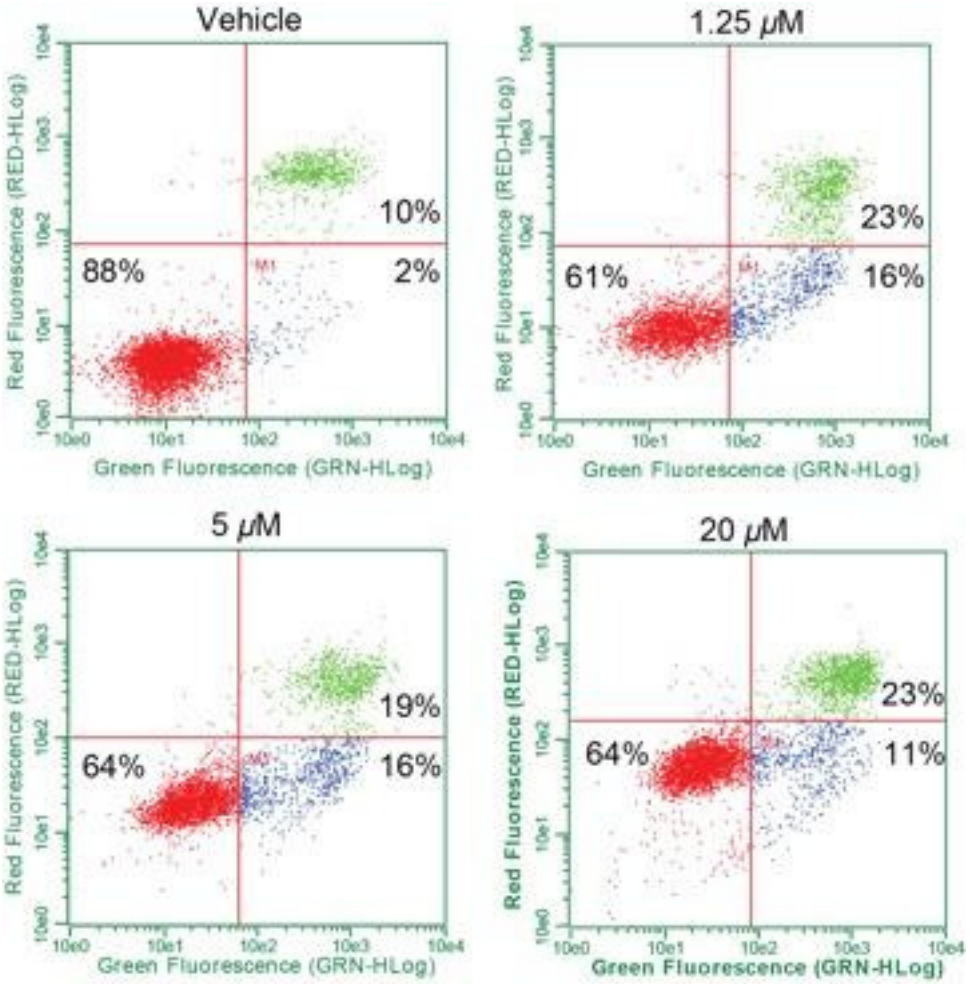

Figure 26. Representative Annexin V flow cytometry data for varying concentrations of Doxorubicin at 24 hours of incubation. Figure courtesy of Dr. Arambula.

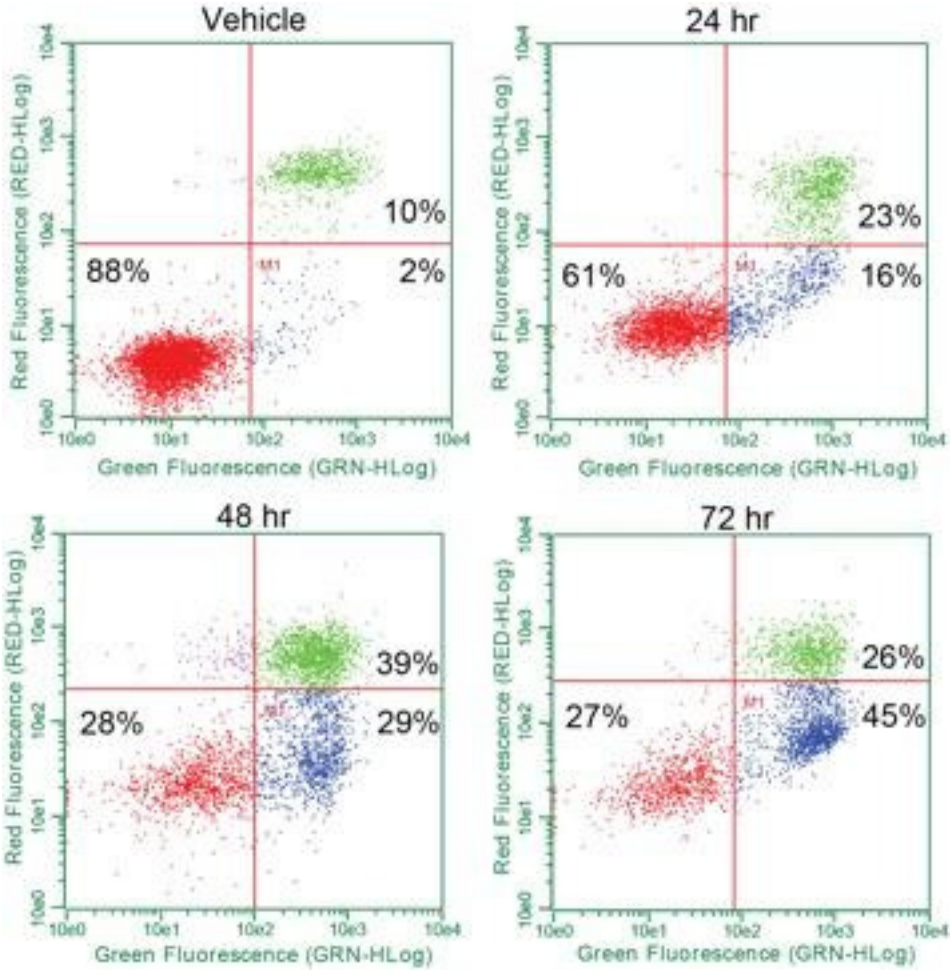

Figure 27. Representative Annexin V flow cytometry data for 1.25μM Doxorubicin after 24, 48, and 72 hours incubation. Figure courtesy of Dr. Arambula.

3.7 DNA Binding as Determined by Thermal Denaturation

Doxorubicin is known to act on cells by intercalating with DNA bases and stopping the function of topoisomerases by keeping the substrate away from the active site of the enzyme.[32] Due to the structural similarities between Doxorubicin and compounds **8** and **9**, the ability of compounds **8** and **9** to bind DNA was evaluated by thermal denaturation studies. The concept behind thermal denaturation is that the temperature required to melt (or separate) a DNA duplex will change in the presence of a compound that affects the stability of the duplex. A compound that stabilizes the duplex will cause the melting temperature to rise above that of the duplex on its own. A compound that destabilizes the duplex will cause the melting temperature to fall below that of the duplex on its own. This change will be visible as a shift to the left or right of a curve showing the absorbance of the duplex at 260 nm at increasing temperatures. The data

collected shows that compounds **8** and **9** have a negligible effect on the melting temperature of the DNA duplex observed, which suggests that they do not bind to DNA. The data does clearly show that Doxorubicin stabilizes the duplex and raises the melting temperature, which is in line with previous literature.[41]

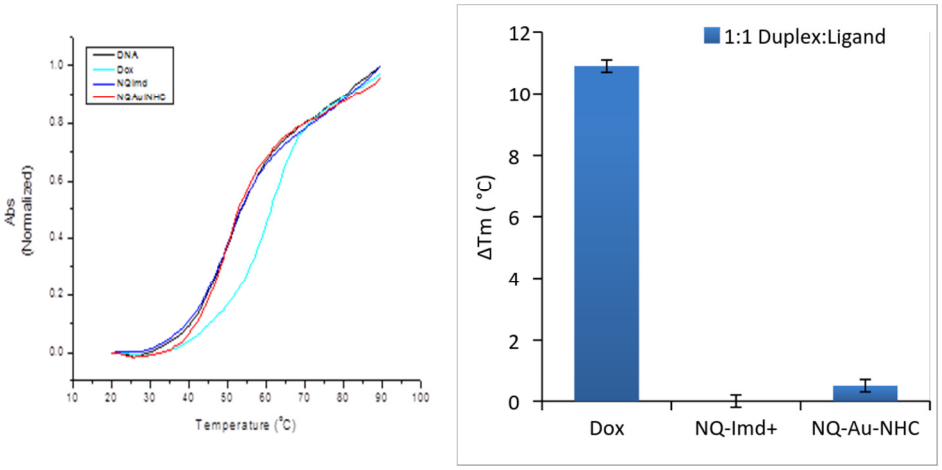

Figure 28. Normalized absorbance of DNA and compound at 260 nm at varying temperatures, and average melting temperatures. NQImd is compound 8, and NQAuNHC is compound 9. Figure courtesy of Zarana Patel.

Chapter 4. Further Mechanistic Elucidation of Compound 6

Work with compounds **1-6** was already in progress when the author joined the Arambula Research Group. The IC_{50} values of these compounds had been established at the University of Texas, and a flow cytometer had already been used to measure intracellular ROS levels in cells exposed to each of Auranofin and compounds **2-6**. Enzymatic activity had also been measured for these compounds. Because the behavior of cells exposed to these compounds has been established by the group, these compounds are used for training purposes for new members of the Arambula Research Group. This also serves to verify the replicability of the work done with these compounds, as the new members of the group are in Georgia, not Texas.

4.1 Zinc Synergy Study

Prior work with ferrocene-functionalized Au-NHC **6** provided evidence that bimodal pathway targeting resulted in greater accentuation of exogenous ROS and increased potency to inhibit cell proliferation. It was also found that A549 cells exposed to compound **6** had higher levels of intracellular chelatable zinc. To this end, cell proliferation assays were conducted on cells from the same original flask of A549 that were dosed with identical concentrations of drug. The only difference between the two plates for each drug would be that one plate per drug would also be treated with 100 μM zinc acetate. After a 3-day incubation, both plates would be dyed with the same dye solution, and the data would be collected and analyzed. The IC_{50} values from each plate would then be statistically evaluated to determine if they were statistically different. In these experiments, Auranofin displayed an IC_{50} value of 1.01 +/- 0.17 μM in A549 cells. The average IC_{50} of Auranofin with 100μM zinc acetate was 0.52 +/- 0.07 μM in A549 cells. When submitted to t-test analysis in GraphPad, the p-value was 0.0271, which is statistically significant. However, when the IC_{50} values of the Auranofin with 100μM zinc acetate are analyzed with the IC_{50} values of every run with Auranofin alone, the difference becomes insignificant (p=0.0604), as the average for every run of Auranofin alone in A549 is 0.92 +/- 0.16 μM. The average IC_{50} value for compound **6** in the presence of 100 μM zinc acetate was 0.127 +/- 0.026 μM, which is not statistically different from the average IC_{50} value of compound **6** without zinc 0.159 +/- 0.017 μM (p=0.3174).

Table 6. P-values of IC_{50} values from the zinc synergy study. Values <0.05 are significant.

	Auranofin	6
Auranofin + 100 µM ZnOAc	0.0271	0.0003
6 + 100 µM ZnOAc	0.0009	0.3174

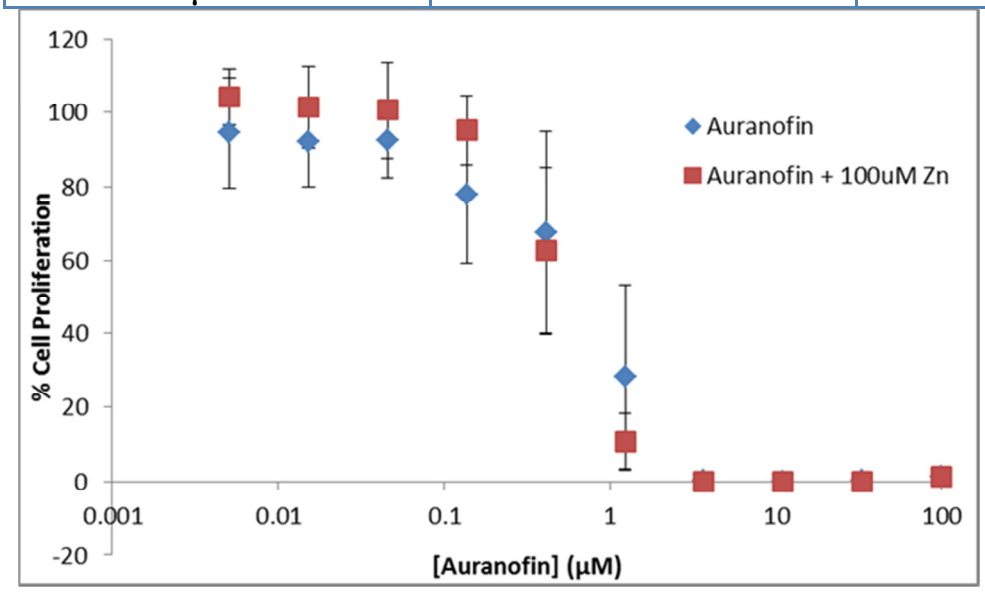

Figure 29. Cell proliferation curves for A549 cells treated with Auranofin alone, and Auranofin in the presence of 100 µM ZnOAc for three days.

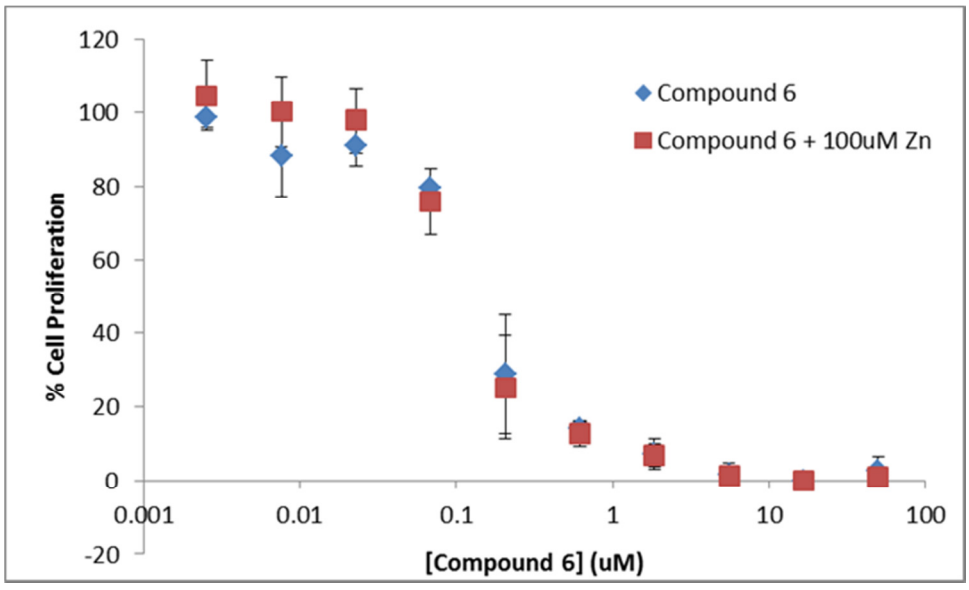

Figure 30. Cell proliferation curves for A549 cells treated with compound 6 alone, and compound 6 in the presence of 100 µM ZnOAc for three days.

Table 7. Average IC50 values of A549

Compound(s)	Average IC_{50} in A549 (µM)	Standard Error
6	0.14	0.03
Auranofin	1.01	0.17
6 + 100 µM ZnOAc	0.127	0.026
Auranofin + 100 µM ZnOAc	0.52	0.07

4.2 Potency in Multiple Cell Lines

The IC_{50} values of compound **6** in A2780, A2780CP, and PC-3 were also determined. These values were 0.194 +/- 0.002 µM, 0.120 +/- 0.003 µM, and 0.475 +/- 0.079 µM, respectively for a 3-day drug incubation. Error here is represented as standard error, but was published as standard deviation in Arambula et al. 2016. Statistical analysis indicated In A2780, compound **6** has about 1.5 fold more anti-proliferative activity than cisplatin and 8 fold more potency than carboplatin. In A2780CP, this difference is 59 fold for cisplatin and 219 fold for carboplatin.[42] There is a 14 fold difference in the IC_{50} value for cisplatin in PC-3 relative to that of compound **6**.[43] Compound **6** is roughly 190 fold more potent in PC-3 than carboplatin.[44]

Table 8. Average IC_{50} values of compound 6 in other cell lines and comparison with literature values for Cisplatin and Carboplatin.

Cell Line	Average IC_{50} of Compound 6 (µM)	Average IC_{50} of Cisplatin (µM)	Average IC_{50} of Carboplatin (µM)
A2780	0.194 +/- 0.002	0.31 +/- 0.06[42]	1.6 +/- 0.3[42]
A2780CP	0.120 +/- 0.003	7.1 +/- 0.09[42]	26.3 +/- 4.1[42]
PC-3	0.475 +/- 0.079	6.6[43]	90[44]

4.3 RNA Isolation for Microarray and Verification of RNA Quality

The QIAgen Protocol for RNA Isolation consistently yielded large quantities of high-purity RNA, as determined by NanoDrop. RNA purity and integrity was visually verified after isolation by gel electrophoresis. Wells that contain genomic DNA will have bands of high molecular weight near the wells, as the DNA will not migrate far. Absence of these bands indicates that the RNA is free of intact genomic DNA. MicroRNA will appear as a faint band or smudge near the far end of the gel, unless it is run completely off the gel. Ribosomal RNA subunits that are intact

will form two distinct bands near the middle of the gel. These bands will be the 28S (closer to the wells) and 18S (closer to the far end of the gel) ribosomal subunits. If these appear as smudges instead of distinct bands, the RNA has been sheared during extraction. Ideally, isolated RNA should be intact, with no DNA contamination or smudging, and have only the bands mentioned above.[45–47] Our gel shows that the RNA isolated by the QIAgen Protocol meets these criteria for purity and integrity (Figures 31 and 32).

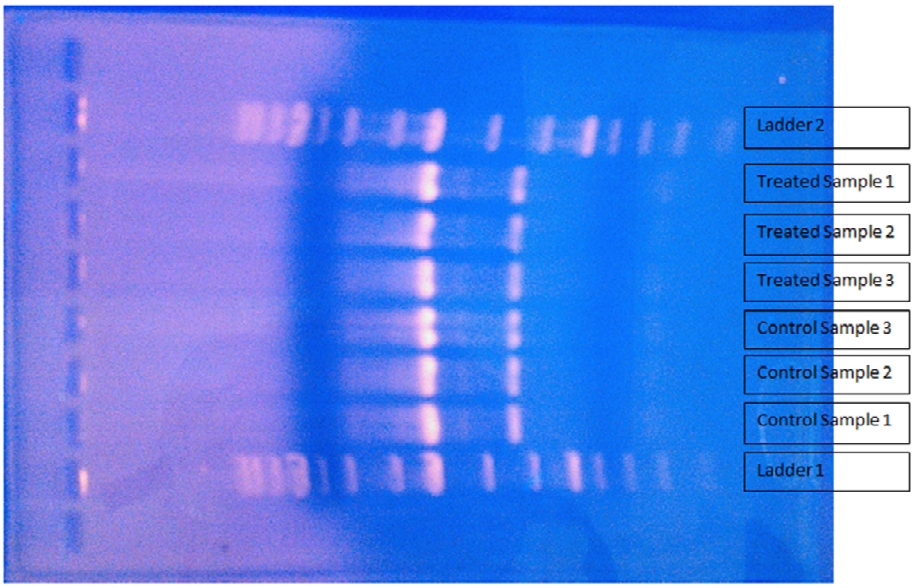

Figure 31. Agarose gel dyed with ethidium bromide and transilluminated with UV light to show RNA sample quality.

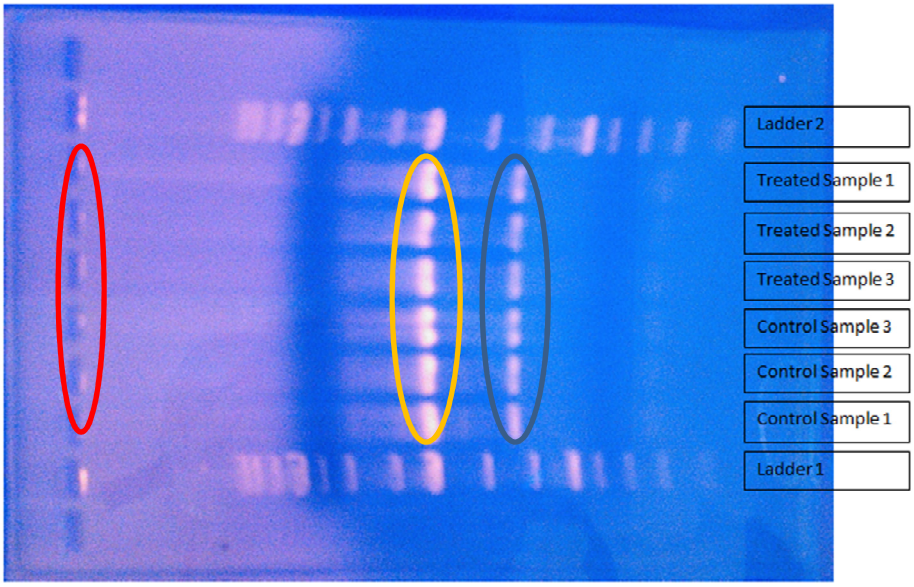

Figure 32. Agarose gel dyed with ethidium bromide and transilluminated with UV light to show RNA sample quality. In the red oval, the absence of genomic DNA can be observed. In the yellow oval, the presence of the 28S ribosomal subunit can be observed. In the blue oval, the presence of the 18S ribosomal subunit can be observed.

4.4 Microarray

Biostatistical analysis (provided by the University of Florida Interdisciplinary Center for Biotechnology Research) yielded 700 differentially-expressed genes in cells treated with 2.5 µM **6** relative to untreated cells. Table 9 shows some of the most note-worthy and most differentially-expressed genes from this group. Several up-regulated genes related to oxidative stress (HMOX1, MT1G, MT1B, MT1H, XBP1, and OSGIN1) were identified in cells treated with **6** relative to cells treated only with vehicle. In addition, several genes related to the Response to ER Stress pathway (CHAC1, DDIT3, TRIB3, ASNS, HERPUD1, ERN1, ATF3, AARS, CXCL8, and HSPA5) were also identified. Another ER-stress response pathway, the Unfolded Protein Response, was upregulated, as well (DDIT3, ASNS, HERPUD1, ERN1, ATF3, AARS, CXCL8, and HSPA5). This result is thought significant, as compounds with similar modes of action to compound **6** are known to localize in the mitochondria.[48] In the case of cells treated with compound **6**, no mitochondria-related gene expression was identified. This data leads us to believe that compound **6** localizes in the endoplasmic reticulum. This prompted the desire for a study of intracellular localization of compound **6**. As seen in Table 10, several genes associated with tRNA synthesis were also differentially expressed between treated and untreated

cells. Several genes related to the p53 pathway and apoptotic signaling were also differentially expressed between treated and untreated cells, as seen in Table 11.

Table 9. Differentially expressed genes between cells treated with 6 and untreated cells. FC is fold change.

Gene ID	Gene symbol	Gene Description	FC	P-value
79094	***CHAC1***	ChaC, cation transport regulator homolog 1	5.56	1.19205E-07
1649	***DDIT3***	DNA-damage-inducible transcript 3	4.43	4.30297E-09
57761	***TRIB3***	tribbles pseudokinase 3 (TRIB3)	4.41	6.5417E-08
440	***ASNS***	asparagine synthetase (glutamine-hydrolyzing)	3.94	3.28201E-08
27063	***ANKRD1***	ankyrin repeat domain 1 (cardiac muscle)	3.90	0.000102275
7779	***SLC30A1***	solute carrier family 30 (zinc transporter)	2.86	0.002992119
23645	***PPP1R15A***	protein phosphatase 1, regulatory subunit 15A	2.79	7.03697E-07
7436	***VLDLR***	very low density lipoprotein receptor	2.56	3.7443E-06
9709	***HERPUD1***	homocysteine-inducible, endoplasmic reticulum stress-inducible, ubiquitin-like domain	2.48	2.53382E-07
2081	***ERN1***	endoplasmic reticulum to nucleus signaling 1	2.44	1.02427E-06
3162	***HMOX1***	heme oxygenase (decycling) 1	2.41	6.63288E-05
4495	***MT1G***	metallothionein 1G	2.24	0.034444693
467	***ATF3***	activating transcription factor 3	2.10	1.231E-06
16	***AARS***	alanyl-tRNA synthetase	2.03	3.39778E-06
2920	***CXCL2***	chemokine (C-X-C motif) ligand 2	1.93	0.00014337
4490	***MT1B***	metallothionein 1B	1.92	0.032952383
3576	***CXCL8***	chemokine (C-X-C motif) ligand 8	1.92	1.10178E-05
7494	***XBP1***	X-box binding protein 1	1.87	3.60972E-05
4496	***MT1H***	metallothionein 1H	1.77	0.025658976
3311	***HSPA7***	heat shock 70kDa protein 7	1.63	0.008645638
6782	***HSPA13***	heat shock protein 70kDa family, member 13	1.54	0.001471724
3309	***HSPA5***	heat shock 70kDa protein 5 (glucose-regulated protein, 78kDa)	1.51	2.83009E-05
29948	***OSGIN1***	oxidative stress induced growth inhibitor 1	1.48	0.000144965
57181	**SLC39A10**	solute carrier family 39 (zinc transporter), member 10	0.63	0.016893383
3306	***HSPA2***	heat shock 70kDa protein 2	0.56	1.49155E-05
6347	***CCL2***	chemokine (C-C motif)	0.39	1.53404E-05

Table 10. Differentially expressed genes between cells treated with 6 and untreated cells that are associated with tRNA synthesis. FC is fold change.

Gene Symbol	Gene Description	FC	P-value
ASNS	asparagine synthetase	1.980	3.28201E-08
GARS	glycyl-tRNA synthetase	1.180	1.23327E-06
CARS	cysteinyl-tRNA synthetase	1.148	2.65564E-07
AARS	alanyl-tRNA synthetase	1.025	3.39778E-06
SARS	seryl-tRNA synthetase	0.947	5.4855E-06
MARS	methionyl-tRNA synthetase	0.901	6.87998E-06
YARS	tyrosyl-tRNA synthetase	0.813	6.23673E-06
TARS	threonyl-tRNA synthetase	0.602	7.61352E-05
EPRS	glutamyl-prolyl-tRNA synthetase	0.580	0.001311123
NARS	asparaginyl-tRNA synthetase	0.568	0.000213934
WARS	tryptophanyl-tRNA synthetase	0.568	0.000373972
IARS	isoleucyl-tRNA synthetase	0.524	4.26376E-05

Table 11. Cell death-associated genes differentially expressed between treated and untreated cells. FC is fold change.

Gene Symbol	Gene Description	FC	P-value
GADD45A	growth arrest and DNA-damage-inducible, alpha	1.000	3.37849E-05
TNFRSF10B	tumor necrosis factor receptor superfamily, member 10b, transcript variant 1	0.645	1.19697E-05
SERPINE1	serpin peptidase inhibitor, clade E	0.668	0.027882965
CCNB1	cyclin B1 interacting protein 1, E3 ubiquitin protein ligase, transcript variant 1	0.562	5.26928E-05
IRAK2	interleukin-1 receptor-associated kinase 2	0.873	5.07967E-05

4.5 Xenografts

Xenografts were prepared of A549 in *Danio rerio* larvae (hatched zebrafish young). As seen in Figure 33, compound **6** was capable of killing the cancerous cells without killing the larvae.

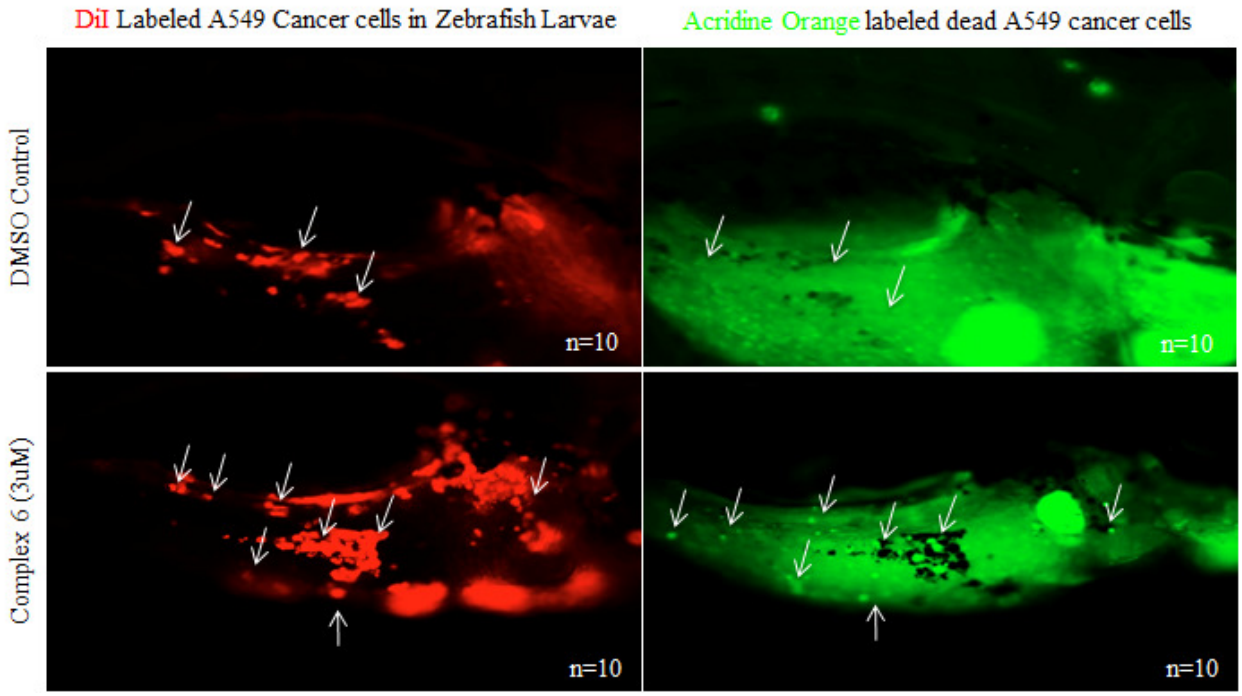

Figure 33. Microscopic images of labelled A549 cells in *Danio rerio* larvae. Figure courtesy of Dr. Sittaramane.

Chapter 5. Discussion

Complex **9** was designed to assess whether the targeting of a network hub (TrxR) in conjunction with an increase of network stress (higher levels of ROS) would lead to a greater alteration in a phenotypic response (cell growth) (cf. Figure 8). The Au(I)-NHC and naphthoquinone moieties were specifically chosen to 1) inhibit TrxR via irreversible binding of Au(I) to the selenothiol-containing active site and 2) accentuate ROS via redox cycling of the naphthoquinone moieties, both within a single molecule. Regarding the ability to inhibit cell proliferation, a substantial increase in potency was observed when considering whole complex **9** compared to Auranofin (23-fold), **8** (~14-fold), or **4** (~10-fold). The latter two compounds (**8**, **4**) provide examples of the individual components of complex **9**. More interestingly, the potency difference between **9** and treatments consisting of an equimolar ratio of **8** and **4** (mimicking that within **9**) suggests a potential synergistic effect when the active moieties are conjugated to create a single complex. The ability to inhibit cell proliferation can often be explained by better understanding cell uptake profiles and potential interactions with extracellular proteins. In consideration of this, it was found by ICP-MS detection of Au that NHC complexes **9** and **4** enter the cell to the same extent, and provided no evidence of interaction with serum proteins. This is in stark contrast to Auranofin, a complex known to bind serum proteins and presumed to enter the cell via protein-assisted uptake; both of which were corroborated by ICP-MS studies reported herein (cf. Figures 15 and 16).

In regards to **9** being able to accentuate intracellular ROS levels, flow cytometry studies in A549 cells indicated a dose-responsive increase in ROS, providing a 27-fold increase at 2.5 μM **9** after a 6-hour incubation. Similar to the cell proliferation studies, the phenotypic alteration/response of the whole complex (i.e. **9**) was greater than the individual components (i.e. **8**, **4**) when compared at all complex concentrations. However, the ROS accentuation difference between **9** and treatments consisting of an equimolar ratio of **8** and **4** (mimicking that within **9**) were statistically similar indicating the lack of synergy regarding the alteration of the ROS phenotype. The inconsistency of synergy between the growth and ROS phenotypes is suggestive of additional mechanisms of action not known at this juncture.

As would be expected from the proposed dual targeting mode of action, complex **9** did inhibit TrxR activity to a greater extent than its individual parts (i.e. **8**, **4**). At low compound

concentration, **9** was found to inhibit TrxR to the same extent as Auranofin (cf. Figure 19), a result not seen in our previous reports.[31] Live cell treatments with a cocktail of **8+4** provided similar TrxR inhibition to that of complex **9**. This evidence suggests that the increased TrxR inhibition by **9** is due to the presence of the naphthoquinone moieties and not due to potential differences in Au-carbene strengths between **9** and **4**.

In considering the design of **9**, large conjugated multi-ring systems are suggestive of potential interactions with nucleic acid based biomolecules. Doxorubicin, a conjugated anthracycline possessing a quinone moiety, is such an example, as its accepted anti-cancer mechanism of action is the inhibition of topoisomerase II via DNA intercalation. However, in healthy cardiac tissue, it has been established that Doxorubicin induces cellular stress and dose-limiting toxicity via mitochondrial ROS accentuation.[49–51] This duplicity is suggestive that similar conjugated systems (such as that seen on the naphthoquinone moieties of **9** and **8**) may elicit a similar mechanism of action. To this effect, thermal denaturation studies with short DNA duplexes were done to elucidate such a mechanism. Significant DNA stabilization by Doxorubicin was evident, however no thermal stabilization of DNA by **9** or **8** was observed under the study conditions. This suggests no interaction with DNA or other nucleic acid based biomolecules with **9** or **8** (Figure 28). Despite the potential differences in biological targets, treatment with complex **9** was found to induce the formation of two positive Annexin-V populations (+PI, -PI), which is indicative of cell death via a controlled apoptotic mechanism (cf. Figure 25). This observation was further corroborated by comparison to results with Doxorubicin known to induce apoptosis (cf. Figures 26 and 27).

To further explore the utility of complex **9** and naphthoquinone **8**, their ability to inhibit cell proliferation was evaluated within a limited panel of cancer cell lines: PC-3 prostate (p53 null), A2780 ovarian (wt-p53, platinum sensitive), and A2780CP (wt-p53, isogenic partner to A2780 displaying multidrug resistance (MDR)). From these results, it should be noted that complex **9** provided enhanced potency within A2780, whereas no significant potency differences were observed between A549, A2780CP, or PC-3. Regarding naphthoquinone **8**, stronger potency was observed in A2780 and PC-3 relative to A2780CP and A549. These trends provide a unique pharmacological profile that warrants further exploration.

To further elucidate the mechanism of **6**, RNA microarray gene expression was conducted. Of the 279 genes that were differentially expressed, a significant number were associated with apoptosis and cell cycle arrest, as might be expected. Gene Ontology (GO) analyses of the transcripts that were differentially-regulated in response to exposure to compound **6** were performed to investigate cellular responses to this complex. Intriguingly, ER stress and oxidative stress response genes were found to be enriched in this analysis. These data, coupled with the differential expression of HMOX1 (containing an antioxidant response element in its promoter) and OSGIN1 (an oxidative response protein that regulates cell death), were taken as an indication that the oxidative stress induced by **6** results in ER stress. The subsequent upregulation of SLC30A1, downregulation of SLC39A10 (both zinc transporters) and upregulation of multiple Metallothioneins are thought to reflect a response to ROS stress, since they serve to attenuate an increase in intracellular zinc concentrations. The role free intracellular (non-protein bound) zinc plays in regulating cellular functions is of considerable relevance to cancer. For example, increased free zinc concentration has been proposed to stabilize hypoxia-inducible factor-1 (HIF-1) and thus influence processes such as glycolysis, apoptosis, and angiogenesis.[52] Moreover, free zinc inhibits thioredoxin reductase,[53] a key mediator in the cellular response to oxidative stress that is frequently overexpressed in cancer.[10,54–59]

The scope and activity of gold complex **6** was further evaluated within a limited panel of cancer cell lines (PC-3 prostate (p53 null), A27780 ovarian (wt-p53 platinum sensitive), and A2780CP (wt-p53 isogenic partner to A2780 displaying multidrug resistance (MDR)) displaying varying p53 status and drug resistance. From these results, it should be noted that there was no observed resistance in A2780CP relative A2780 cell lines. This result is considered significant in that small molecular platinum-containing species often display 2-27 fold resistance between this isogenic pair.[3,42]

Compounds **6** and **9** were shown to be lethal to *Danio rerio* embryos at all concentrations of 10nM or higher. Further studies into intracellular localization of **6** and possibly **9** by confocal microscopy and/or mitochondrial extraction are planned. Xenografts of A549 and PC-3 into *Danio rerio* embryos to study the *in vivo* effects of compounds **6** and **9** are in progress, but not yet completed. Preliminary results suggest that compound **6** is effectively killing the xenografted cells without killing the host.

At 2.5 μM, all of the experimental compounds studied except compound **11** were shown to disrupt antioxidant activity by protein inhibition and increase intracellular ROS. The experimental compounds were also shown to have high anticancer potency by the MTT assay. These results are supportive of the hypothesis that multimodal pathway targeting will result in enhancement in phenotypic alterations that are controlled by said pathway.

Chapter 6. Materials and Methods

6.1 Materials

Cell culture media consisted of RPMI 1640 with 2 mM glutamine and 25 mM HEPES (Corning 10041cv), with 10% heat-inactivated fetal bovine serum (RMBIO FBS-BBT) and 1X penicillin-streptomycin (Sigma p4333). Unless otherwise noted, incubators were set to 37 °C and 5% CO_2. Trypsin (HyClone SH30236.01) and 1X Phosphate Buffered Saline (HyClone SH30258.02, diluted in autoclaved deionized water) were used for general cell line maintenance and harvesting. Cell lines were obtained from the ATCC (A549 and PC-3) and Prof. Zahid Siddik at the M.D. Anderson Cancer Center (A2780 and A2780CP). Cell culture plastic ware consisted of generic T-75 flasks, treated 6-well plates, treated 96-well plates, large treated dishes, and cell scrapers (Fisher 353085).

Compounds **1-11** were synthesized by Dr. Kuppuswamy Arumugam at Wright State University.[31] Auranofin (Tocris Bioscience 4600) was used as a control in enzymatic studies. Stock solutions of complexes **1-11** and Auranofin were made in DMSO (2.5 mM-10 mM, depending on the compound and its solubility). Doxorubicin (Tocris Bioscience 2252) was used as a control in cell proliferation assays and intracellular ROS studies, and stock solutions were 5 mM in DMSO. Cisplatin (Acros Organics 193762500) stock solutions were 5 mM in 100 mM NaCl (Carolina 88-8880) in deionized water. Cisplatin and zinc acetate stock solutions were then sterile filtered using a 0.2 µm syringe filter (Fisher 973019). Zinc acetate (Baker 4296) was used for zinc synergy studies, and its stock solutions were 5 mM in autoclaved deionized water.

Thiazolyl blue tetrazolium bromide (Alfa Aesar L11939) was used for cell proliferation assays. A Molecular Devices SpectraMax 190 UV-vis plate reader was used to record the absorbance values for the MTT cell proliferation assay, the lipoate reduction assay for Thioredoxin Reductase activity, and the Modified Lowry assay.

Trace Metal Grade acids for use with the ICP-MS were HCl (Fisher A508-4) and HNO_3 (Sigma 225711-475mL). Diluent for samples and standards run on the ICP-MS was a 3% HCl solution made with the Trace Metal Grade HCl and autoclaved deionized water. The Inductively-Coupled Plasma Mass Spectrometer used was a Perkin Elmer NexION 300X set to detect gold at 197 m/z. Gold concentrations were quantified using the linear range of a standard curve

generated by serial dilution of an ICP-MS gold standard (Ricca MSAU1KH-100) in 3% HCl. Values were then normalized to protein content as determined using a Modified Lowry Protein Assay Kit (Thermo 23240) and known concentrations of bovine serum albumin (Fisher 9048-46-8). The Lowry Assays were performed in round bottomed 96-well clear plates (Fisher 12565500). The stir table used for mixing Lowry samples was a Lab-Line Instruments, Inc. 3520 Orbit Shaker. The settings used were the maximum settings that allowed the plate to remain on the table.

Fetal bovine serum (HyClone SH30910.02) that was not heat-inactivated was used for protein binding studies after being warmed to roughly 37 °C.

The activity of Thioredoxin Reductase was monitored in live cells using a solution of lipoate (Tokyo Chemical Industry Co., Ltd. L0207) and DTNB (Acros Organics 117540050) in 1X HBSS (Life tech 14025-092). If insufficient lipoate was dissolved, this will become evident by curvature of the graph of the normalized lipoate reduction over time after reagent introduction. This graph should be practically linear for all treatments over the entire course of the experiment. It can be seen in Figures 19, 20, 22, 23, 33, 34, 45, and 46 that these graphs were linear for all treatments tested in our lab.

The QIAgen Protocol for RNA Isolation utilized a QIAgen RNeasy Plus Universal Mini Kit. RNA concentrations were determined using a Thermo Scientific NanoDrop 2000c Spectrophotometer. RNA quality was visually verified using ethidium bromide and an agarose gel. Agarose (IBI Molecular Biology Certified IB70070) was dissolved in autoclaved 1X TAE buffer (diluted from BIORAD 50X TAE buffer), spiked with 12 µL of 10 mg/mL ethidium bromide, and cast using a Fisher FB-SB-710 gel electrophoresis chamber. The ladder used was a Thermo SM1331 Generuler 1kb Plus DNA Ladder.

For the flow cytometry, CM-H_2DCFDA (Lifetech C6827) was used for the determination of relative intracellular ROS, and propidium iodide (Chemodex P0023) was used to exclude dead cells from the population of interest. An FITC Annexin V Apoptosis Detection Kit (BD Biosciences 556547) was used for determining whether the compounds were acting by apoptosis or necrosis. The flow cytometer used was a Millipore Guava easyCyte8 working in conjunction with Guava inCyte software.

Thermal melt data was obtained using duplex DNA from IDT with complementary sequences 5'CCGCAGCCA3' and 5'TGGCTGCGG3'. The instrument used was a Shimadzu 2600 UV-vis spectrophotometer equipped with an 8-cell microcell (b= 1.0 cm, 130 µL total volume) and a thermal melt apparatus.

A549 and PC-3 cells were prepared for injections into *Danio rerio* embryos to form a xenograft model in which to study the in vivo effects of compounds **6** and **9** on tumors formed by these cell lines. RPMI 1640 (Just Media) was used during the dye process. The dye used to track the cells once in the fish was Vybrant DiI Cell Labeling Solution (LifeTech V22889).

6.2 Assay Overview and Design

Several well-established assays were used to evaluate the biological activity of our compounds in cancer cell models. The MTT assay is a colorimetric assay in which a water-soluble tetrazolium dye is introduced to cells, and allowed to incubate for 4 hours. During the incubation, the thiazolyl blue tetrazolium bromide (yellow) enters the cell. If the cells are alive and actively proliferating, the mitochondrial enzymes of the cell will react with the dye to form purple water-insoluble formazan crystals. The crystals remain in the cell and can be observed microscopically at the end of the incubation. After removal of the liquid in the plate that the experiment was conducted in, the cells and crystals can be solubilized in DMSO, and the absorbance at 570 nm can be recorded. This can then be used to determine relatively what percentage of cells in each treatment group was actively proliferating. The data can be graphed as percent cell proliferation vs. concentration of compound in the well, and then fit with curve-fitting software to determine the IC_{50} of the compound in the cell line under those conditions. The IC_{50} value is a measure of the anti-proliferative potency of the compound. It is the concentration at which half of the cells are proliferating, and half of them are not. Important variables to note when comparing IC_{50} values are the length of cell exposure to the compound, the cell line used, and literature values of other compounds under the same conditions.[20,61,62]

The lipoate reduction assay is commonly used to measure the activity of the antioxidant enzyme thioredoxin reductase *in vitro*. It offers a way of assessing the effects of a compound on the upper threshold of ROS homeostasis in the cell. After incubating the cells in the desired concentrations of compound for a few hours, the media is removed and replaced with a solution

of lipoate and DTNB reagent in isotonic buffer. The absorbance of the wells at 405 nm is then observed periodically for several hours. During this time, the lipoate enters the cells. Intracellular thioredoxin reductase then reduces the lipoate, forming dihydrolipoate. Dihydrolipoate is then excreted from the cell, where it can interact with extracellular DTNB, causing a color change from a pale yellow to a much more intense yellow.[6,9] The data from this can be graphed in many ways, which will be discussed later.

Intracellular levels of ROS can be quantified by flow cytometric analysis with the help of CM-H_2DCFDA and propidium iodide (PI). CM-H_2DCFDA is a fluorescein-based dye that has been modified with acetate groups, such that the dye will not react with reactive oxygen species found outside the cell. After entering the cell, the acetate groups are cleaved by intracellular enzymes, allowing the dye to react with intracellular reactive oxygen species. The product of this reaction fluoresces green.[5] Propidium iodide is a fluorescent dye that cannot permeate the cell membrane. However, propidium iodide intercalates with nucleic acids, which changes its excitation and emission wavelengths. As a cell dies, the membrane becomes permeable to the propidium iodide, and other dyes used to indicate cell death. This allows the researcher to exclude dead cells from the population of cells with high green fluorescence, so that only live cells are studied.[63]

A microarray was used to measure differential gene expression in treated and untreated cells. This technique is well-established, but costly. In the procedure, live cells are lysed, and their mRNA is isolated. The purity, concentration, and quality of the mRNA is assessed, and then hybridized with a fluorescent dye. Samples from treated cells are hybridized with one dye, while samples from untreated cells are hybridized with another dye (usually, one is red, and the other is green). The samples are then washed over a chip with affixed DNA sequences that correspond to specific genes. If the mRNA encounters a complementary DNA sequence, it will form a duplex. Excess mRNA is then washed off of the chip, and the fluorescence of both dyes is recorded for each position on the chip. The data is run through a computer, which is programmed to know what gene was encoded at each position. A biostatistician can interpret the data and report what genes are being expressed differentially and what the difference in expression is between the two groups.[64]

6.3 Cell Proliferation by MTT Assay

Cells were harvested and seeded into 96-well culture plates (Costar 07-200-90) in 100 µL of culture media. They were allowed to incubate overnight at 37 °C in the presence of 5% CO_2. A549 was seeded at a density of 1000 cells/well, A2780 at 2500 cells/well, A2780CP at 3000 cells/well, and PC-3 at 2000 cells/well. The next day, appropriate serial dilutions of drug stocks in culture media were made. 100 µL of the appropriate solution was then added to each well of the 96-well plate. The final concentration of DMSO in these solutions was not permitted to exceed 10% of the solution. Cells were then placed into the incubator for three days, before being dyed with 50 µL/well of 3 mg/mL MTT dye in serum-free RPMI 1640 and incubated for another 4 hours. The liquid was then removed from the plates by vacuum aspiration. The remaining cells and formazan crystals were dissolved in 50 µL/well DMSO. The absorbance of the wells at 570 nm was then recorded using a Molecular Devices SpectraMax 190 UV-vis plate reader. The average absorbance of the wells with dead cells as determined by microscopic observation was subtracted from the average absorbance of all other treatments. The average absorbance of wells with live, happily proliferating cells was defined as 100% cell proliferation. The average percent cell proliferation per treatment was then determined, and the IC_{50} values were determined using the non-linear curve-fitting tool on Origin. IC_{50} values were compared on GraphPad by the unpaired t-test, with a confidence interval of 95%. A significant difference in values is shown by a p-value less than 0.05 in this confidence interval. A p-value of 0.01 or below is seen as a much more significant difference, with a much higher confidence interval.

6.4 Cellular Uptake as Determined by Lowry Assay and ICP-MS

Cells were grown up to 70-80% confluence in T-75 cell culture flasks (Thermo 130190). Cells were then washed with 8 mL 1X warm PBS. 2 mL 1X PBS was then added to each flask, and the cells were removed by scraping. Each cell suspension was then pipetted into a clean, labeled 15 mL centrifuge tube (Thermo 339650). Cells were pelleted by centrifuging at 1000 rpm for 5 minutes in an Eppendorf 5804 with a swing-bucket rotor. The supernatant was removed by vacuum aspiration, and the pellet was resuspended in 50 µL autoclaved deionized water. Suspension/lysates were then kept at -80 °C. After thawing, the lysates were then sonicated using a Branson Digital Sonifier, and 5 µL aliquots were taken for determination of protein content of the sample. Lysates were digested with 80 µL aqua regia and heated to 65 °C

for one hour. Digested lysates were diluted with 4 mL 3% Trace Metal Grade HCl and gold content was measured by ICP-MS.

The Modified Lowry Assay was used to determine the protein content of each sample for normalization purposes. The standard curve for each run was made from a 2-fold serial dilution of fresh 5 mg/mL BSA solution. Aliquots were diluted to within the linear range of the standard curve using autoclaved DI water, and subjected to the Modified Lowry Assay in a 96-well plate. Each well contained 10 µL of sample, 50 µL of Modified Lowry Reagent, and 5 µL of 1N Folin-Ciocalteau Reagent. All other aspects of the procedure were as detailed in the microplate procedure instructions that come with the kit.[65]

6.5 Serum Protein Binding Study

The binding of gold from each compound to proteins in fetal bovine serum were observed during a time-dependent study. A 25 µM solution of each compound in 3 mL warm FBS was made. The solutions were kept at 37 °C. Over time, 100 µL aliquots of each solution were taken and precipitated into 400 µL cold methanol. Precipitated aliquots were stored at -80 °C. The methanolic suspensions were then centrifuged at 13000 rcf for 5 minutes in an Edvotek microcentrifuge. The supernatants were pipetted into new microcentrifuge tubes. Samples were prepared for ICP-MS by adding 200 µL supernatant from each sample to 2 mL 3% Trace Metal Grade HCl. Time points were at addition of compound (T0), 4, 6.25, 9.75, 12, 24, 48, 72, and 100 hours.

6.6 Determination of Intracellular ROS

In Texas, 1 million cells/well of A549 were seeded into a 6-well plate in culture media and allowed to adjust overnight in the incubator. The next day, cells were treated with 0.625-2.5 µM compound. Control cells were treated with DMSO in culture media. After incubating for 6 hours, the liquid was removed by vacuum aspiration and the cells were washed with PBS. Cells were then treated with 250 µL trypsin and incubated for 5-15 minutes, after which they were collected into a tube. Cells were centrifuged for 3 minutes at 300 rcf at 5 °C. The supernatant was removed by vacuum aspiration. Then, the cells were washed twice with cold PBS, and centrifuged again at 300 rcf for 3 minutes at 5 °C. The supernatant was discarded again. The cells were resuspended at a density of 1 million cells/mL in fresh 2 µM CM-H_2DCFDA in PBS. After this, they were

incubated in the dark for 15 minutes, and centrifuged again to pellet the cells. Then, the supernatant was discarded, the cells were washed with 2 mL of PBS, and the cells were resuspended in 2 µg/mL propidium iodide in PBS at a density of 0.5 million cells/mL. Controls included cells dyed only with propidium iodide, cells dyed only with CM-H_2DCFDA, and unstained cells. Each sample was then pipetted into 1 well of a 96-well plate, and submitted to FACS analysis.

6.7 Inhibition of Intracellular Thioredoxin Reductase by Lipoate Reduction Assay

Cells were harvested and seeded at a density of 10000 cells/well A549 in 96-well culture plates. They were then incubated overnight at 37 °C and 5% CO_2. The next day, appropriate serial dilutions of drug stock in culture media were performed, and 100 µL of the appropriate solution were added to each well. Cells were returned to the incubator for 6 hours. Afterwards, the liquid was then removed from each well by vacuum aspiration and replaced by 100 µL of 5 mM lipoate and 1 mM DTNB in HBSS. The absorbance of each well at 605 nm was recorded immediately and once every 20 minutes for three hours. Plates were covered with aluminum foil between readings. The average absorbance of each treatment at T_0 was subtracted from the average absorbance of that same treatment at all other time points. The average absorbance of the control wells at 180 minutes after addition of the lipoate-DTNB reagent was defined as 1, and all other data points were normalized to that value. Data is presented by dose of compound, by the compound used over all doses used, and by compound used over time after addition of the lipoate-DTNB reagent, along with standard error.

6.8 Determination of Cell Death Pathway by FITC Annexin V

An FITC Annexin-V Apoptosis Detection Kit from BD Biosciences was used to determine whether cells exposed to various compounds were dying by apoptotic pathways or by necrosis. In Texas, 200,000-300,000 cells of A549 were seeded into each well of a 6-well plate in culture media and allowed to adjust overnight in the incubator. The next day, cells were treated with 1.25-20 µM drug in culture media and incubated for 24 hours. Control cells were treated with DMSO in culture media. After the incubation, the media from each well was collected. The cells were washed with PBS, and the wash was also collected. Half-strength trypsin in PBS was introduced to the cells, and the cells were incubated for 2 minutes. The loosened cells were

pooled with their respective collected media and PBS wash, and then centrifuged at 300 rcf for 3 minutes. The supernatant was discarded, and the cells were washed twice with cold PBS. The cells were centrifuged again at 300 rcf for 3 minutes. The supernatant was discarded, and the cells were resuspended in Annexin V binding buffer at a density of 1 million cells/mL. A 100 µL aliquot of each sample was then placed into a new microcentrifuge tube. Each sample was then treated with 5 µL Annexin V and 50 µg/mL propidium iodide solution. Controls included unstained cells, cells stained with just Annexin V, and cells stained with just propidium iodide. Cells were incubated in the dark for 15 minutes at ambient temperature, and then diluted with 200 µL Annexin V binding buffer. After this, each sample was placed into 1 well of a 96-well plate and submitted to FACS analysis.

6.9 DNA Binding as Determined by Thermal Denaturation

The ability of doxorubicin, compound 8, and compound 9 to alter the stability of a DNA duplex was determined by thermal denaturation performed by Zarana Patel. Stock solutions of 1.6 mM DNA were made in 1X TE buffer and stored at 5 °C. When duplex DNA was needed, equimolar amounts of the complementary strands were mixed and incubated at 95 °C for 5 minutes, then chilled on ice. Tubes were then centrifuged to collect any condensate. The resulting solution was aliquoted into microcentrifuge tubes, and 1 molar equivalent of compound was added to each tube. Each tube then received 12 µL 1 mM EDTA, 12 µL 100 mM NaCl, 12 µL 20 mM MOPS buffer pH 7.4, and sufficient diluent for a final volume of 120 µL/sample. This yielded a final DNA and compound concentration of 5 µM. Each sample was placed into one well of the 8-microcell cuvette, and run through the Shimadzu 2600 UV-vis thermal melt apparatus. The samples were heated to 95 °C from 20 °C at 1 °C/minute. The resulting data was then run through Origin (a program from MicroCal) to determine the maximum of the first derivative of the curve.

6.10 RNA Isolation for Microarray and Verification of RNA Quality

The QIAgen Protocol was used to isolate RNA from untreated cells and cells treated with compound **6** prior to use for microarray. About 5 million A549 cells in 11 mL of culture media were seeded into each of two large treated culture dishes per replicate. For each replicate, cells used were from the same original flask and passage. The cells were then returned to the

incubator and allowed to sit overnight. The next morning, control cells were given 11 mL more culture media, while treated cells were given 11 mL of 5 μM compound 6 in culture media, for a final concentration of 2.5 μM. After incubating for 6 hours, the liquid in each dish was removed by vacuum aspiration. The cells were then washed with 5 mL warm PBS, then incubated with 2.5 mL trypsin for 5 minutes. The trypsin was then quenched with 10mL culture media, and the cells were collected into centrifuge tubes by pipetting. Cells were centrifuged at 1000 rpm for 5 minutes in an Eppendorf 5804 with a swing-bucket rotor, and then the supernatant was removed by vacuum aspiration. Each pellet was resuspended in 380 μL PBS, and then transferred to a microcentrifuge tube. Each sample was lysed by adding 900 μL QIAzol Lysis Reagent and homogenized by vigorous shaking and vortexing. The QIAgen RNeasy Plus Universal Mini Total RNA protocol was then picked up at Step 4.[66] Finally, RNA was eluted in a total of 60 μL RNase-free water. RNA was stored at -80°C, and RNA concentrations were checked by NanoDrop, usually in triplicate. RNA samples that were obtained by the QIAgen Protocol were run on a 1% agarose gel spiked with ethidium bromide in 1X TAE buffer at 125 V for 1 hour, alongside a dsDNA ladder. About 1400 ng of each sample was run per well, with 1X sample loading dye (BIORAD 1660401). Afterwards, the gel was de-stained with water for 10 minutes, and photographed with a Kyocera Brigadier while being transilluminated with UV light.

6.11 Preparation for Microarray

After being run on an agarose gel and deemed intact RNA, RNA samples (400 ng + 3 μL) were sent to the Interdisciplinary Center for Biotechnology Research at the University of Florida for microarray analysis. The microarray used was an Affymetrix GeneChip Human Transcriptome 2.0 Array. A biostatistician at UF was paid to further analyze the data.

6.12 Xenografts in *Danio rerio*

A549 cells were harvested, and aliquots of 1 million cells in suspension were placed into microcentrifuge tubes. A total of about 4 million cells were used for each round of the experiment. The cells were centrifuged at 500 rcf for 2.5 minutes, and the supernatant was discarded. Cells were resuspended in 1 mL of RPMI 1640 per tube. Each tube was then dyed with 5 μL DiI solution and mixed well. The cells were then incubated for 15 minutes. After this, the tubes were centrifuged at 500 rcf for 2.5 minutes again. The supernatant was discarded, and

the cells were resuspended in 200 µL culture media per tube. At this point, cells were walked over to Dr. Sittaramane's lab in the Biological Sciences Building for injection into *Danio rerio* embryos that had been prepared in advance as described in Sittaramane and Abid et al. 2015.[67]

Chapter 7. Conclusion

Herein we report that the targeting of an antioxidant network hub (TrxR) results in a greater phenotypic alteration (cell proliferation) when combined with a component capable of inducing network stress (i.e. accentuation of oxidative stress via redox cycling). The proposed incorporation of a redox cycling center within the Au(I)-NHC core provided an enhancement in anti-proliferative activity, ROS accentuation, and the inhibition of TrxR activity when compared to individual components, thus providing an additional "proof-of-principle" example for the suggestion that it is useful to address key cancer-related pathways via multiple modes of targeting. Differential gene expression analysis of A549 lung cells treated with ferrocene-incorporated variants (i.e. **6**) suggested that the exogenous ROS accentuation was inducing ER Stress and UPR pathways. It has recently been suggested that activation of such stress pathways could lead to the immunogenic cell death in vivo.[60] Accordingly, further mechanistic studies, tests of toxicity and efficacy in mammalian models, as well as efforts to prepare and test second-generation complexes that are able to accentuate ROS effects via multiple pathways are underway. The results of these efforts will be presented in due course.

References

1. Arora S, Kothandapani A, Tillison K, Kalman-Maltese V, Patrick SM. Downregulation of XPF-ERCC1 Enhances Cisplatin Efficacy in Cancer Cells. *DNA Repair (Amst)*. 2010;9(7):745-753. doi:1.1016.j.dnarep.2010.03.010.

2. Florea E, Busselberg D. Cisplatin as an Anti-Tumor Drug: Cellular Mechanisms of Drug Resistance and Induced Side Effects. *Cancers (Basel)*. 2011;3(1):1351-1371. doi:10.3390/cancers3011351.

3. Arambula JF (Georgia SUD of C, Sessler JL, Siddik ZH. A Texaphyrin-oxaliplatin Conjugate That Overcomes Both Pharmacologic and Molecular Mechanisms of Cisplatin Resistance in Cancer Cells. *Medchemcomm*. 2012;3(10):1275-1281.

4. Sies H. Oxidative stress: oxidants and antioxidants. *Exp Physiol*. 1997;82(2):291-295. doi:10.1113/expphysiol.1997.sp004024.

5. Linux N, Media R. Detection of Intracellular Reactive Oxygen Species. *Bio-protocol*. 2013;3:67-68.

6. Nordberg J, Arnér ESJ. Reactive oxygen species, antioxidants, and the mammalian thioredoxin system. *Free Radic Biol Med*. 2001;31(11):1287-1312. doi:10.1016/S0891-5849(01)00724-9.

7. Ray PD, Huang B, Tsuji Y. Reactive Oxygen Species (ROS) homeostasis and redox regulation in cellular signaling. *Cell Signal*. 2012;24(5):981-990.

8. Berners-Price SJ, Filipovska A. Gold Compounds as Therapeutic Agents for Human Diseases. *Metallomics*. 2011;3:863-873. doi:10.1039/c1mt00062d.

9. Rackham O, Shearwood AMJ, Thyer R, et al. Substrate and inhibitor specificities differ between human cytosolic and mitochondrial thioredoxin reductases: Implications for development of specific inhibitors. *Free Radic Biol Med*. 2011;50(6):689-699. doi:10.1016/j.freeradbiomed.2010.12.015.

10. Lincoln DT, Al-Yatama F, Mohammed FMA, et al. Thioredoxin and thioredoxin reductase expression in thyroid cancer depends on tumour aggressiveness. *Anticancer Res*. 2010;30(3):767-776.

11. Karlenius TC, Tonissen KF. Thioredoxin and Cancer: A Role for Thioredoxin in all States of Tumor Oxygenation. *Cancers (Basel)*. 2010;2(2):209-232.

12. Kim HJ, Chae H-Z, Kim Y-J, et al. Preferential Elevation of Prx I and Trx expression in lung cancer cells following hypoxia in human lung cancer tissues. *Cell Biol Toxicol*. 2003;19(5):285-298.

13. Bey-Liing M, Powis G. INHIBITION OF CELLULAR THIOREDOXIN REDUCTASE BY DIAZIQUONE AND DOXORUBICIN: Relationship to the inhibition of cellular proliferation and decreased ribonucleotide reductase activity. 1992;43(7):1621-1626.

14. Bey-Liing M, Powis G. Inhibition of thioredoxin reductase (E.C. 1.6.4.5.) by antitumor quinones. *Free Radic Res*. 1990;8:365-372. doi:10.3109/10715769009053370.

15. ATCC. A549 (ATCC CCL-185). http://www.atcc.org/Products/All/CCL-185.aspx#generalinformation. Accessed June 13, 2015.

16. Honma M, Hayashi M, Ohno T, Mizusawa H, Saijo K, Sofuni T. Heterogeneity of the Y Chromosome Following Long-Term Culture of the Human Lung Cancer Cell Line A549. *Vitr Cell Dev Biol*. 1996;32(5):262-264. http://limk.springer.com/article/10.1007/BF02723057#page-1.

17. Meng X, Wang X, Wang Y. More than 45% of A549 and H446 cells are cancer initiating cells: evidence from cloning and tumorigenic analyses. *Oncol Rep*. 2009;21(4):995-1000.

18. Soussi T. *Handbook of p53 Mutation in Cell Lines*. 1.0 ed.; 2007.

19. Sigma Aldrich. A2780. http://www.sigmaaldrich.com/catalog/product/sigma/93112519?lang=en&region=US. Accessed June 14, 2016.

20. Bodo J, Chovancova J, Hunacova L, Sedlak J. Enhanced sensitivity of human ovarian carcinoma cell lines A2780 and A2780 / CP to the combination of cisplatin and synthetic isothiocyanate ethyl 4-isothiocyanatobutanoate. *Neoplasma*. 2005;52(6):510-516.

21. Public Health England. ECACC General Cell Collection: A2780. http://www.phe-culturecollections.org.uk/products/celllines/generalcell/detail.jsp?refId=93112519&collection=ecacc_gc. Accessed June 14, 2016.

22. Zendehel R, Masoudi-Nejad A, Mohammadzadeh J, Shirazi FH. Cisplatin Resistant Patterns in Ovarian Cell Line Using FTIR and Principle Component Analysis. *Iran J Pharm Res*. 2012;11(1):235-240.

23. Jacob F, Nixdorf S, Hacker NF, Heinzelmann-Schwartz VA. Reliable in vitro studies require appropriate ovarian cancer cell lines. *J Ovarian Res*. 2014;1(60). doi:10.1186/1757-2215-7-60.

24. ATCC. PC-3 (ATCC CRL-1435). http://www.atcc.org/Products/All/CRL-1435.aspx#generalinformation. Accessed June 13, 2015.

25. Occhipinti G, Jensen VR, Tornroos KW, Froystein NA, Bjorsvik H-R. Synthesis of a New Bidentate NHC Ag(I) Complex and its Unanticipated Reaction with the Hoveyda-Grubbs First Generation Catalyst. *Tetrahedron*. 2009;65:7186-7194.

26. Samantaray MK, Dash C, Shaikh MM, Pang K, Butcher RJ, Ghosh P. Gold(III) N-heterocyclic Carbene Complexes Mediated Synthesis of beta-Enaminones From 1,3-Dicarbonyl Compounds and Aliphatic Amines. *Inorg Chem*. 2011;50:1840-1848.

27. Arumugam K, Varnado CD, Sproules S, Lynch VM, Bielawski CW. Redox-switchable ring-closing metathesis: catalyst design, synthesis and study. *Chem-Eur J*. 2013;19:10866-10875.

28. Howarth J, Thomas JL, Hanlon K, McGuirk D. 1,3-Di(Ferrocenylmethyl)Imidazolium and 1-Ferrocenylmethyl-3-alkylimidazolium Salts: A High Yield and Facile Synthesis. *Synth Commun*. 2000;30:1865-1878.

29. Hashmi ASK, Hengst T, Lothschutz C, Rominger F. New and Easily Accessible Nitrogen Acylic Gold(I) Carbenes: Structure and Application in the Gold-Catalysed Synthesis as well as the Hydration of Alkynes. *Adv Synth Catal*. 2010;352:1315-1337.

30. Flahaut A, Roland S, Mangeney P. Allylic Alkylation and Amination Using Mixed (NHC)(phosphine) palladium Complexes Under Biphasic Conditions. *J Organomet Chem*. 2007;692:5754-5762.

31. Arambula JF, McCall R, Sidoran KJ, et al. Targeting antioxidant pathways with ferrocenylated N-heterocyclic carbene supported gold(I) complexes in A549 lung cancer cells. *Chem Sci*. 2016;7(2):1245-1256. doi:10.1039/C5SC03519H.

32. Poornima P, Kumar VB, Weng CF, Padma VV. Doxorubicin induced apoptosis was potentiated by neferine in human lung adenocarcima, A549 cells. *Food Chem Toxicol*. 2014;68:87-98. doi:10.1016/j.fct.2014.03.008.

33. Biosciences BD. No Title. http://www.bdbiosciences.com/eu/applications/research/apoptosis/apoptosis-kits-sets/fitc-annexin-v-apoptosis-detection-kit-i/p/556547. Accessed May 12, 2016.

34. El-Najjar N, Ketola RA, Nissilä T, et al. Impact of protein binding on the analytical detectability and anticancer activity of Thymoquinone. *J Chem Biol*. 2011;4(3):97-107. doi:10.1007/s12154-010-0052-4.

35. Ferraro G, Gabbiani C, Merlino A. First Crystal Structure for a Gold Carbene–Protein Adduct. *Bioconjug Chem*. 2016:acs.bioconjchem.6b00298. doi:10.1021/acs.bioconjchem.6b00298.

36. Vairetti M, Ferrigno A, Bertone R, Richelmi P, Bertè F, Freitas I. Apoptosis vs. necrosis: Glutathione-mediated cell death during rewarming of rat hepatocytes. *Biochim Biophys Acta - Mol Basis Dis*. 2005;1740(3):367-374. doi:10.1016/j.bbadis.2004.11.022.

37. Jordan D, Hindocha S, Dhital M, Saleh M, Khan W. The Epidemiology, Genetics, and Future Management of Syndactyly. *Open Orthop J*. 2012;6:14-27. doi:10.2174/1874325001206010014.

38. Liu J, Akahoshi T, Namai R, Matsui T, Kondo H. Effect of Auranofin, an antirheumatic drug, on neutrophil apoptosis. *Inflamm Res*. 2000;49(9):445-451. http://www.ncbi.nlm.nih.gov/pubmed/11071118.

39. Fan C, Zheng W, Fu X, Li X, Wong Y-SS, Chen T. Enhancement of Auranofin-Induced Lung Cancer Cell Apoptosis by Selenocysteine, a Natural Inhibitor of TrxR1 in vitro and in vivo. *Cell Death Dis*. 2014;5(4):e1191-11. doi:10.1038/cddis.2014.132.

40. Hoyt MT, Palchaudhuri R, Hergenrother PJ. Cribrostatin 6 Induces Death in Cancer Cells Through a Reactive Oxygen Species (ROS)-mediated Mechanism. *Invest New Drugs*. 2010;29(4):562-573. doi:10.1007/s10637-010-9390-x.

41. Rabbani A, Sharoghi B, Khodabandeh M. Interaction of Doxorubicin with DNA-HMG1 Complex. *J Sci I R Iran*. 1995;6(3):147-152.

42. Arambula JF, Sessler JL, Siddik ZH. Overcoming biochemical pharmacologic mechanisms of platinum resistance with a texaphyrin-platinum conjugate. *Bioorganic Med Chem Lett*. 2011;21(6):1701-1705. doi:10.1016/j.bmcl.2011.01.092.

43. Marques J, Silva VLM, Silva AMS, Marques MPM, Braga SS. Ru(II) trithiacyclononane 5-(2-hydroxyphenyl)-3-[(4-methoxystyryl)pyrazole], a complex with facile synthesis and high cytotoxicity against PC-3 and MDA-MB-231 cells. *Complex Met*. 2014;1:7-12.

44. Ibrahim SRM, Mohamed GA, Shaala LA, Youssef DTA. Calotroposide S, New Oxypregnane Oligoglycoside from Calotropis procera Root Bark. *Rec Nat Prod*. 2016;10(6):761-765.

45. Agarose Gel Electrophoresis and RNA. ThermoFisher Scientific. https://www.thermofisher.com/us/en/home/references/protocols/nucleic-acid-purification-and-analysis/rna-protocol/agarose-gel-electrophoresis-of-rna.html. Published 2016. Accessed July 13, 2016.

46. Is Your RNA Intact? Methods to Check RNA Integrity. ThermoFisher Scientific. https://www.thermofisher.com/us/en/home/references/ambion-tech-support/rna-isolation/tech-notes/is-your-rna-intact.html. Published 2016. Accessed July 13, 2016.

47. RNA Analysis on Non-Denaturing Agarose Gel Electrophoresis. Evrogen. http://evrogen.com/technologies/RNA-electrophoresis.shtml. Published 2016. Accessed July 13, 2016.

48. Spreckelmeyer S, Orvig C, Casini A. Cellular Transport Mechanisms of Cytotoxic Metallodrugs: An Overview Beyond Cisplatin. *Molecules*. 2014;19:15584-15610. doi:10.3390/molecules191015584.

49. Simunek T, Sterba M, Popelova O, Adamcova M, Hrdina R, Gersl V. Anthracycline-induced cardiotoxicity: overview of studies examining the roles of oxidative stress and free cellular iron. *Pharmacol Rep*. 2009;61(1):154-171. http://www.ncbi.nlm.nih.gov/pubmed/19307704.

50. Kim S-Y, Kim S-J, Kim B-J, et al. Doxorubicin-induced reactive oxygen species generation and intracellular Ca2+ increase are reciprocally modulated in rat cardiomyocytes. *Exp Mol Med*. 2006;38(5):535-545. doi:10.1038/emm.2006.63.

51. Wang S, Konorev EA, Kotamraju S, Joseph J, Kalivendi S, Kalyanaraman B. Doxorubicin induces apoptosis in normal and tumor cells via distinctly different mechanisms. Intermediacy of H(2)O(2)- and p53-dependent pathways. *J Biol Chem*. 2004;279(24):25535-25543. doi:10.1074/jbc.M400944200.

52. Wei W-H, Fountain M, Magda D, et al. Gadolinium texaphyrin-methotrexate conjugates. Towards improved cancer chemotherapeutic agents. *Org Biomol Chem*. 2005;3(18):3290-3296. doi:10.1039/B503664J.

53. Magda D, Lecane P, Miller RA, et al. Motexafin gadolinium disrupts zinc metabolism in human cancer cell lines. *Cancer Res*. 2005;65(9):3837-3845. http://cancerres.aacrjournals.org/cgi/doi/10.1158/0008-5472.CAN-04-4099.

54. Schumacker PT. Reactive oxygen species in cancer cells: live by the sword, die by the sword. *Cancer Cell*. 2006;10(3):175-176. doi:10.1016/j.ccr.2006.08.015.

55. Diehn M, Cho RW, Lobo NA, et al. Association of reactive oxygen species levels and radioresistance in cancer stem cells. *Nature*. 2009;458(7239):780-783. doi:10.1038/nature07733.

56. Trachootham D, Alexandre J, Huang P. Targeting cancer cells by ROS-mediated mechanisms: a radical therapeutic approach? *Nat Rev Drug Discov*. 2009;8(7):579-591. doi:10.1038/nrd2803.

57. Gorrini C, Harris IS, Mak TW. Modulation of oxidative stress as an anticancer strategy. *Nat Rev Drug Discov*. 2013;12(12):931-947. doi:10.1038/nrd4002.

58. Berggren M, Gallegos A, Gasdaska JR, Gasdaska PY, Warneke J, Powis G. Thioredoxin and thioredoxin reductase gene expression in human tumors and cell lines, and the effects of serum stimulation and hypoxia. *Anticancer Res*. 1996;16(6B):3459-3466. http://www.ncbi.nlm.nih.gov/pubmed/9042207.

59. Raffel J, Bhattacharyya AK, Gallegos A, et al. Increased expression of thioredoxin-1 in human colorectal cancer is associated with decreased patient survival. *J Lab Clin Med*. 2003;142(1):46-51. doi:10.1016/S0022-2143(03)00068-4.

60. Terenzi A, Pirker C, Keppler BK, Berger W. Anticancer metal drugs and immunogenic cell death. *J Inorg Biochem*. 2016. doi:10.1016/j.jinorgbio.2016.06.021.

61. Hiwasa T, Utsumi T, Yasuraoka M, et al. Functional Similarity of Anticancer Drugs by MTT Bioassay. *J Cancer Sci Ther*. 2011. omicsonline.org/functional-similarity-of-anticancer-drugs-by-mtt-bioassay-1948-5956.1000099.php?aid=3119.

62. Osibote E, Noah N, Sadik O, McGee D. Electrochemical Sensors, MTT and Immunofluorescence Assays for Monitoring the Efeects of Cissus populnea Extracts on Sertoli Cells. *Reprod Biol Endocrinol*. 2011;9. http://www.rbej.com/content/9/1/65.

63. ThermoFisher Scientific. Propidium Iodide - 1.0mg/mL Solution in Water. https://www.thermofisher.com/order/catalog/product/P3566. Accessed June 18, 2016.

64. Klug WS, Cummings MR, Spencer CA, Palladino MA. Genetic Analysis Using Gene Expression Microarrays. In: Wilbur B, Carlson G, Friedman D, Early M, eds. *Essentials of Genetics*. 7th ed. Benjamin Cummings; 2010:418-421.

65. Instructions: Modified Lowry Protein Assay Kit. 2011.

66. *RNeasy Plus Universal Handbook*. QIAGEN; 2010.

67. Sittaramane V, Padgett J, Salter P, et al. Discovery of Quinoline-Derived Trifluoromethyl Alcohols, Determination of Their in vivo Toxicity and Anticancer Activity in a Zebrafish Embryo Model. *ChemMedChem*. 2015;10:1802-1807.

Appendix

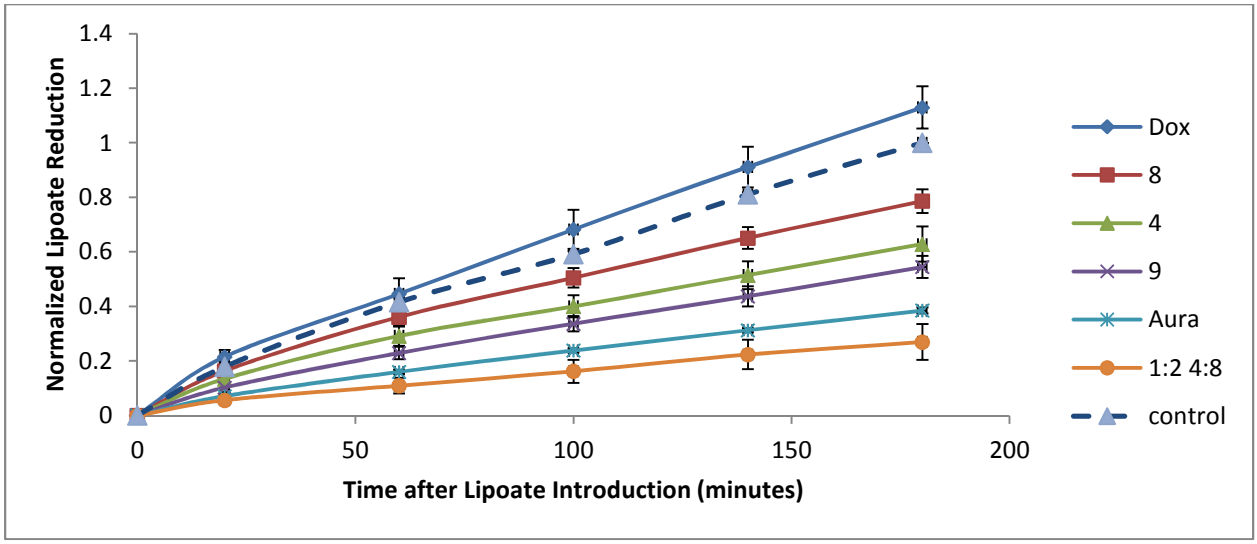

Figure 34. Normalized lipoate reduction with standard error in A549 over 3 hours, after 6 hours incubation in 2.5 µM compound.

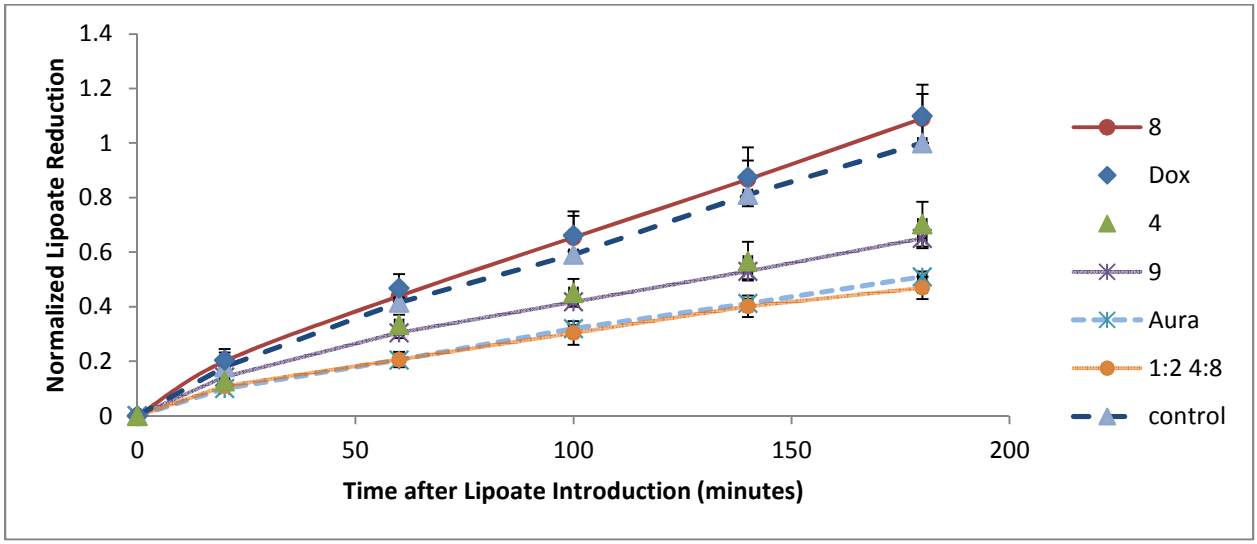

Figure 35. Normalized lipoate reduction with standard error in A549 over 3 hours, after 6 hours incubation in 1.25 µM compound.

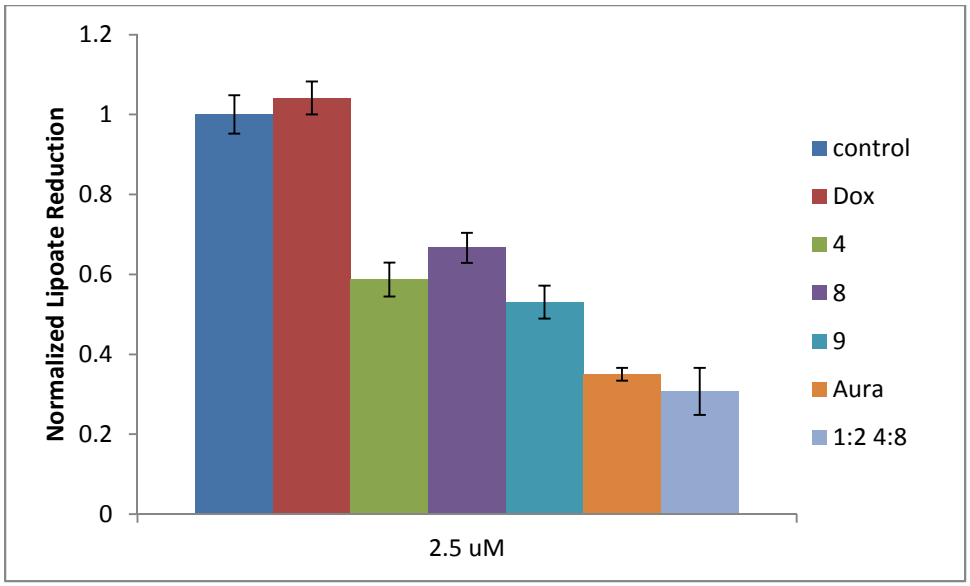

Figure 36. Normalized lipoate reduction and standard error in A549 at 2.5 µM compound, 180 minutes after addition of lipoate.

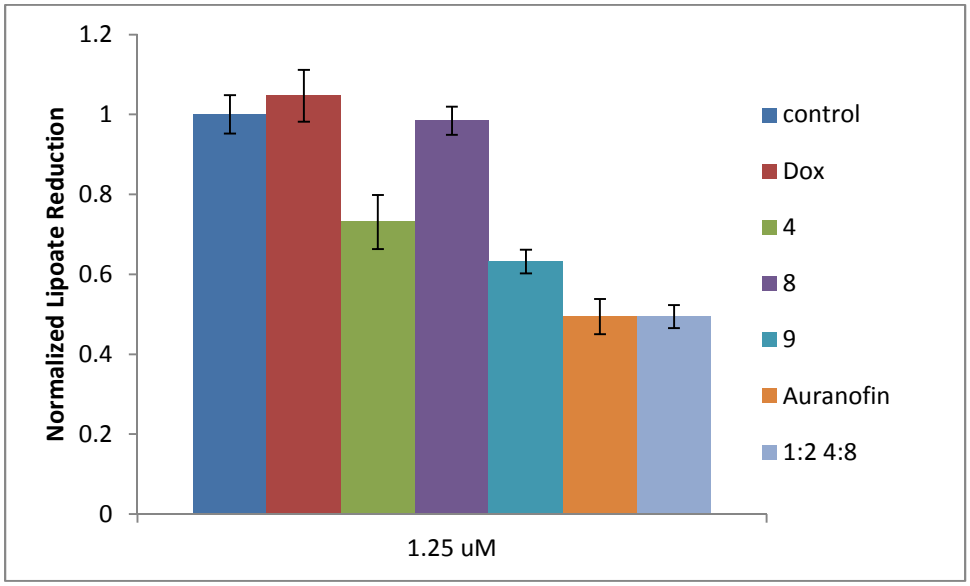

Figure 37. Normalized lipoate reduction and standard error in A549 at 1.25 µM compound, 180 minutes after addition of lipoate.

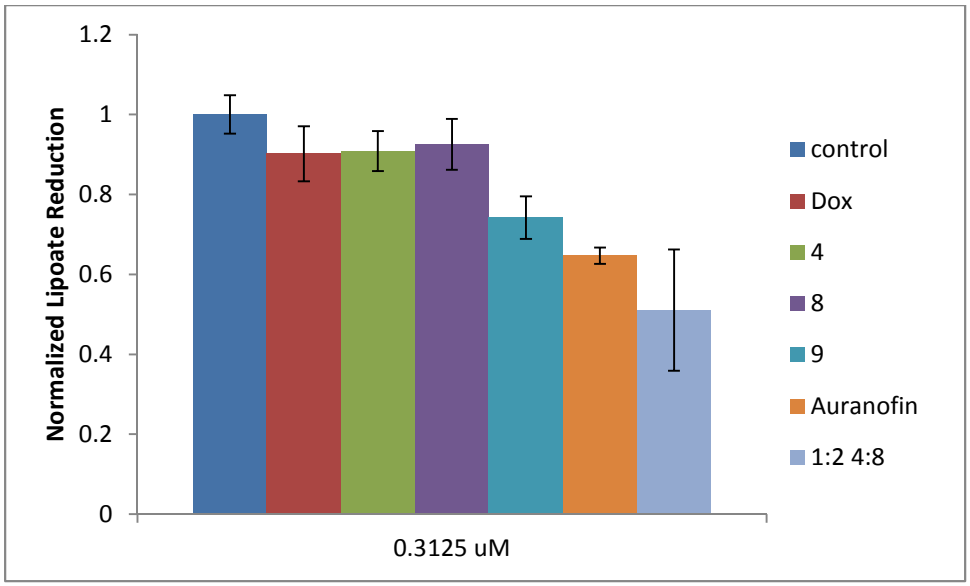

Figure 38. Normalized lipoate reduction and standard error in A549 at 0.3125 µM compound, 180 minutes after addition of lipoate.

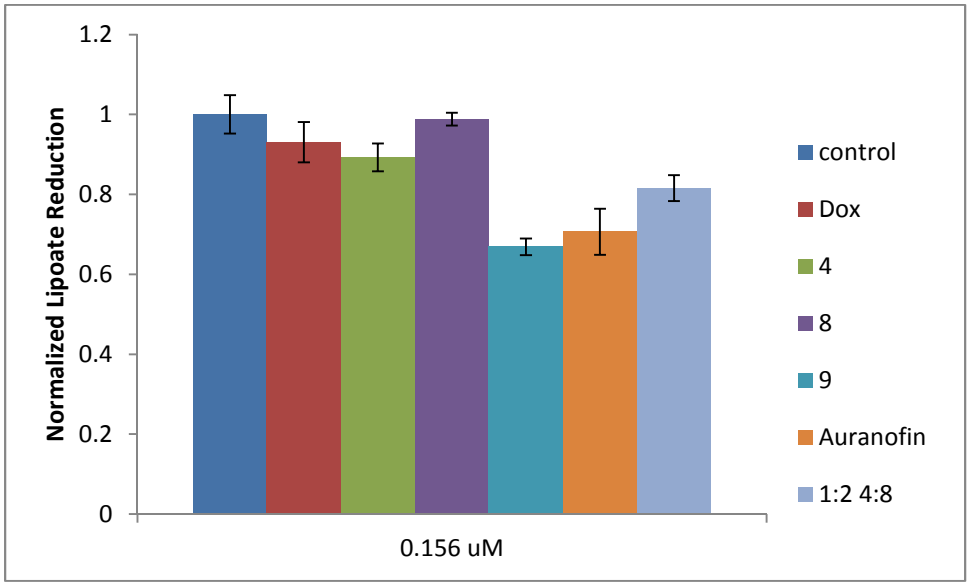

Figure 39. Normalized lipoate reduction and standard error in A549 at 0.156 µM compound, 180 minutes after addition of lipoate.

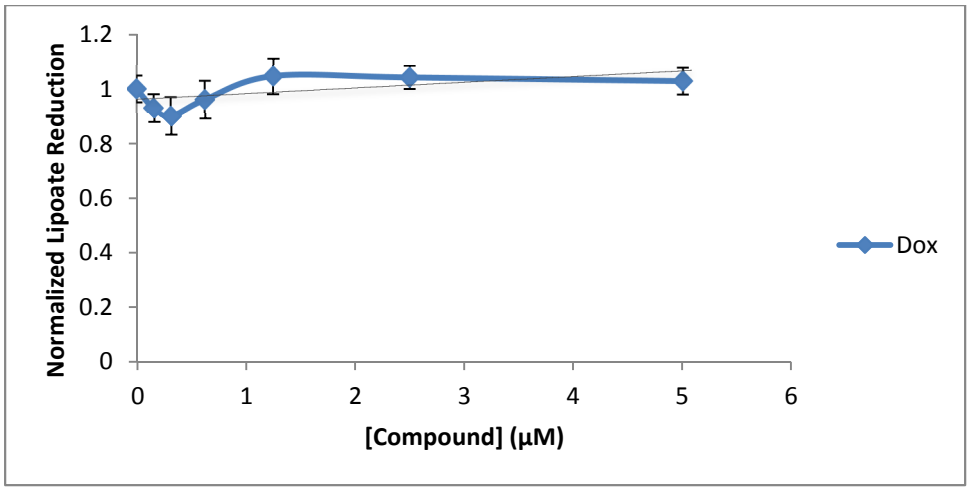

Figure 40. Normalized lipoate reduction and standard error in A549 at varying concentrations of Doxorubicin, 180 minutes after addition of lipoate.

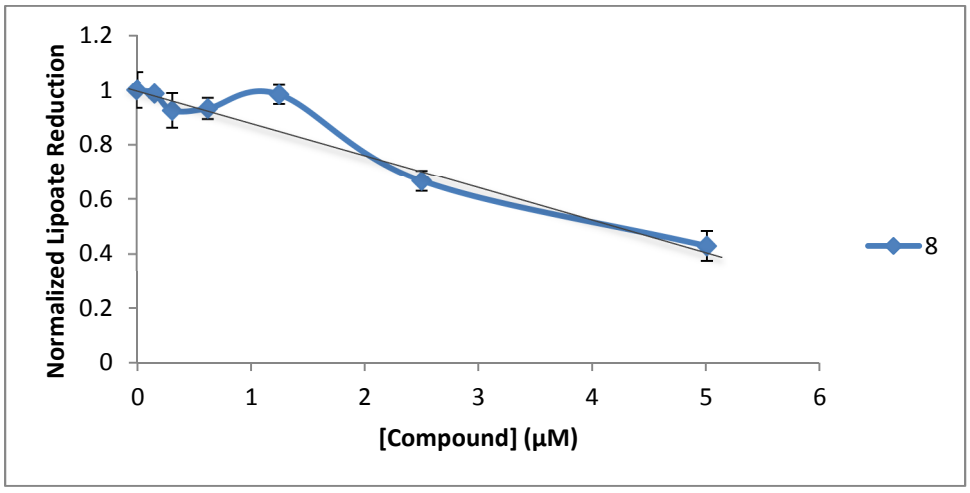

Figure 41. Normalized lipoate reduction and standard error in A549 at varying concentrations of compound 8, 180 minutes after addition of lipoate.

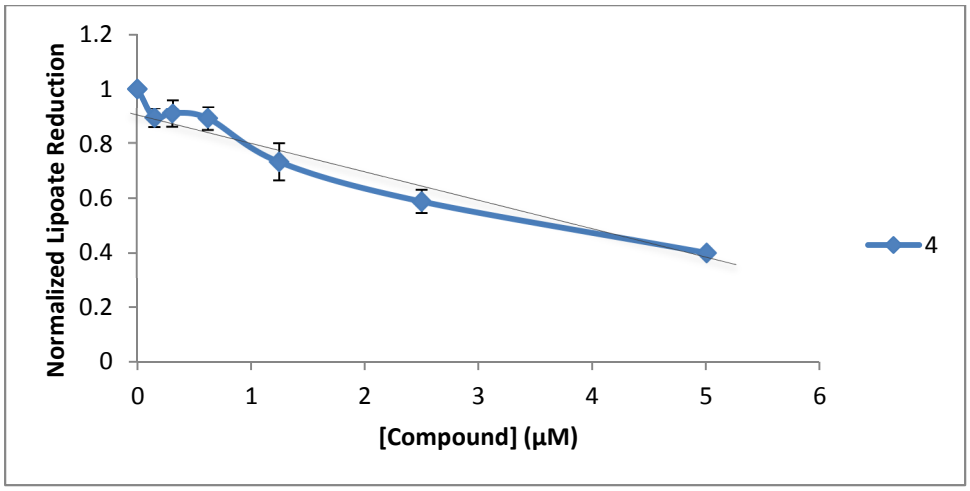

Figure 42. Normalized lipoate reduction and standard error in A549 at varying concentrations of compound 4, 180 minutes after addition of lipoate.

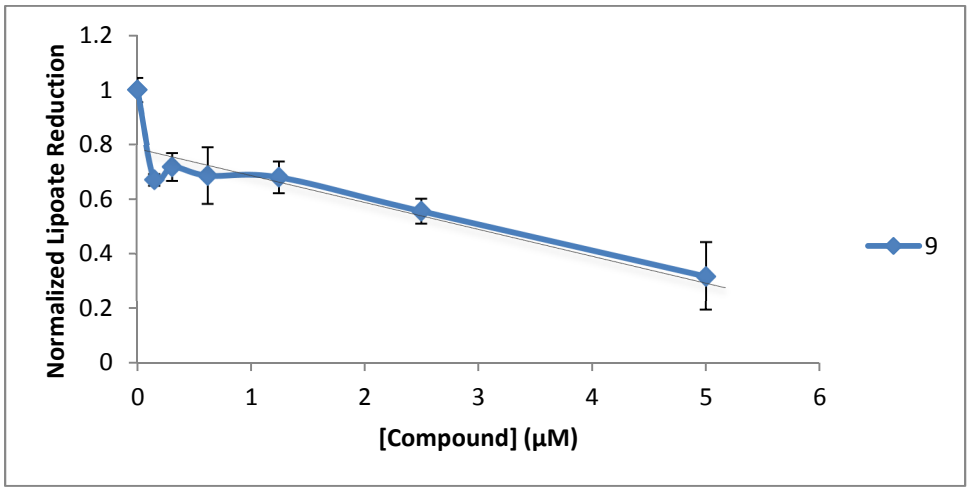

Figure 43. Normalized lipoate reduction and standard error in A549 at varying concentrations of compound 9, 180 minutes after addition of lipoate.

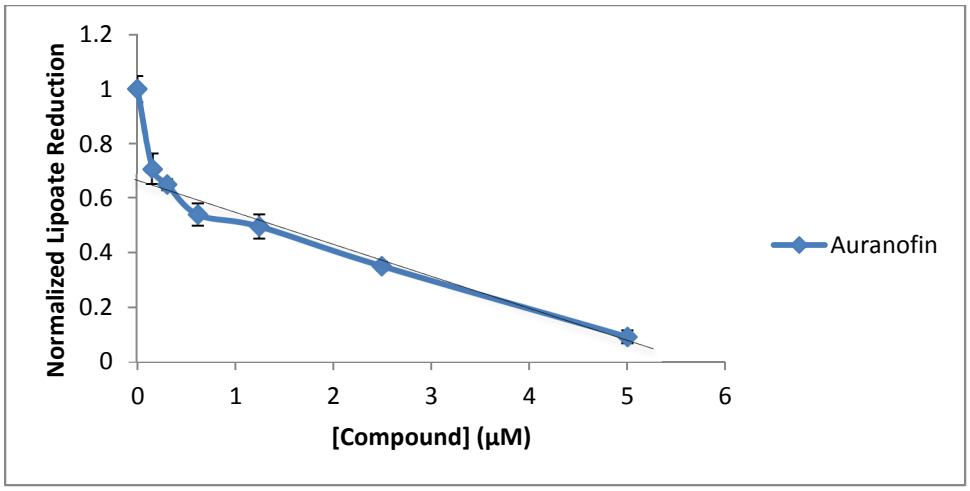

Figure 44. Normalized lipoate reduction and standard error in A549 at varying concentrations of Auranofin, 180 minutes after addition of lipoate.

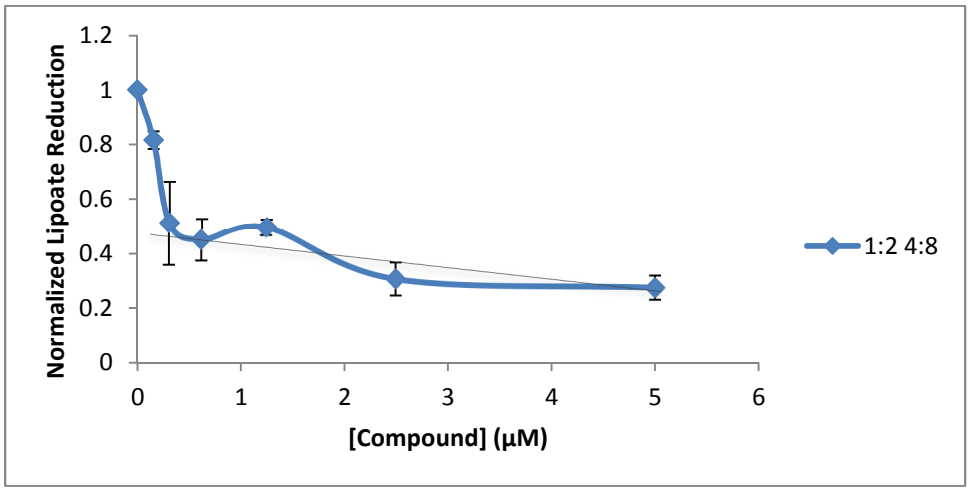

Figure 45. Normalized lipoate reduction and standard error in A549 at varying concentrations of 1:2 4:8 cocktail, 180 minutes after addition of lipoate.

Table 12. P-values of t-tests comparing normalized lipoate reduction resulting from varying concentrations of compound to that of the same concentration of other compounds. Values less than 0.05 are significant.

Compound	[Compound] (μM)	Control	Dox	8	4	9	Aura	1:2 4:8
Dox	0.15625	0.0898	---	0.3529	0.5699	0.0330	0.0436	0.1019
	0.3125	0.1083	---	0.8214	0.9483	0.1566	0.0114	0.0574
	0.625	0.5855	---	0.7219	0.4286	0.0021	0.0002	0.0012
	1.25	0.4910	---	0.4200	0.0105	0.0004	<0.0001	0.0002
	2.5	0.3402	---	<0.0001	<0.0001	<0.0001	<0.0001	<0.0001
	5	0.4007	---	0.0011	0.0002	0.0001	<0.0001	0.0003
8	0.15625	0.3506	0.3529	---	0.1420	0.0017	0.0092	0.0080
	0.3125	0.2189	0.8214	---	0.8792	0.1214	0.0089	0.0484
	0.625	0.1170	0.7219	---	0.4972	0.0003	<0.0001	0.0002
	1.25	0.6652	0.4200	---	0.0097	<0.0001	<0.0001	<0.0001
	2.5	<0.0001	<0.0001	---	0.2151	0.0378	<0.0001	0.0006
	5	<0.0001	0.0011	---	0.6344	0.0225	0.0046	0.0908
4	0.15625	0.0204	0.5699	0.1420	---	0.0824	0.1263	0.2963
	0.3125	0.1276	0.9483	0.8792	---	0.1491	0.0087	0.0895
	6.25	0.0481	0.4286	0.4972	---	0.0019	0.0001	0.0013
	1.25	0.0067	0.0105	0.0097	---	0.2491	0.0140	0.0306
	2.5	<0.0001	<0.0001	0.2151	---	0.3868	0.0005	0.0069
	5	<0.0001	0.0002	0.6344	---	0.0031	0.0003	0.0502
9	0.15625	<0.0001	0.0330	0.0017	0.0824	---	0.6656	0.0463
	0.3125	0.0012	0.1566	0.1214	0.1491	---	0.1465	0.2714
	0.625	<0.0001	0.0021	0.0003	0.0019	---	0.2895	0.1176
	1.25	<0.0001	0.0004	<0.0001	0.2491	---	0.0186	0.0136
	2.5	<0.0001	<0.0001	0.0378	0.3868	---	0.0015	0.0151
	5	<0.0001	0.0001	0.0225	0.0031	---	0.0283	0.2734
Aura	0.15625	0.0001	0.0436	0.0092	0.1263	0.6656	---	0.1338
	0.3125	<0.0001	0.0114	0.0089	0.0087	0.1465	---	0.4080
	0.625	<0.0001	0.0002	<0.0001	0.0001	0.2895	---	0.2627
	1.25	<0.0001	<0.0001	<0.0001	0.0140	0.0186	---	0.9995
	2.5	<0.0001	<0.0001	<0.0001	0.0005	0.0015	---	0.4107
	5	<0.0001	<0.0001	0.0046	0.0003	0.0283	---	0.0200
1:2 4:8	0.15625	0.0014	0.1019	0.0080	0.2963	0.0463	0.1338	---
	0.3125	0.0182	0.0574	0.0484	0.0895	0.2714	0.4080	---
	0.625	0.0004	0.0012	0.0002	0.0013	0.1176	0.2627	---
	1.25	<0.0001	0.0002	<0.0001	0.0306	0.0136	0.9995	---
	2.5	<0.0001	<0.0001	0.0006	0.0069	0.0151	0.4107	---
	5	<0.0001	0.0003	0.0908	0.0502	0.2734	0.0200	---

Table 13. P-values of t-tests comparing normalized lipoate reduction of varying concentrations of compound to that of other concentrations of the same compound. Values less than 0.05 are significant.

Compound	[Compound] (μM)	0.15625	0.3125	0.625	1.25	2.5	5
Dox	0.15625	---	0.7466	0.7963	0.2990	0.1632	0.2502
	0.3125	0.7466	---	0.5709	0.1769	0.0997	0.2224
	0.625	0.7963	0.5709	---	0.3888	0.3403	0.5455
	1.25	0.2990	0.1769	0.3888	---	0.9503	0.8597
	2.5	0.1632	0.0997	0.3403	0.9503	---	0.8496
	5	0.2502	0.2224	0.5455	0.8597	0.8496	---
8	0.15625	---	0.4796	0.3585	0.9161	0.0007	0.0006
	0.3125	0.4796	---	0.9209	0.4320	0.0076	0.0034
	0.625	0.3585	0.9209	---	0.3525	0.0006	0.0001
	1.25	0.9161	0.4320	0.3525	---	0.0001	<0.0001
	2.5	0.0007	0.0076	0.0006	0.0001	---	0.0084
	5	0.0006	0.0034	0.0001	<0.0001	0.0084	---
4	0.15625	---	0.8755	0.9860	0.2661	0.0155	0.0021
	0.3125	0.8755	---	0.8235	0.1618	0.0073	0.0021
	0.625	0.9860	0.8235	---	0.1084	0.0018	0.0003
	1.25	0.2661	0.1618	0.1084	---	0.1388	0.0157
	2.5	0.0155	0.0073	0.0018	0.1388	---	0.0247
	5	0.0021	0.0021	0.0003	0.0157	0.0247	---
9	0.15625	---	0.4423	0.3830	0.5043	0.1063	0.0015
	0.3125	0.4423	---	0.0977	0.1153	0.0245	0.0014
	0.625	0.3830	0.0977	---	0.5365	0.2941	0.0008
	1.25	0.5043	0.1153	0.5365	---	0.0804	<0.0001
	2.5	0.1063	0.0245	0.2941	0.0804	---	0.0016
	5	0.0015	0.0014	0.0008	<0.0001	0.0016	---
Aura	0.15625	---	0.3088	0.0284	0.0139	<0.0001	0.0006
	0.3125	0.3088	---	0.0363	0.0121	<0.0001	<0.0001
	0.625	0.0284	0.0363	---	0.3987	0.0004	<0.0001
	1.25	0.0139	0.0121	0.3987	---	0.0039	0.0002
	2.5	<0.0001	<0.0001	0.0004	0.0039	---	<0.0001
	5	0.0006	<0.0001	<0.0001	0.0002	<0.0001	---
1:2 4:8	0.15625	---	0.0959	0.0043	0.0003	0.0003	0.0002
	0.3125	0.0959	---	0.7326	0.9198	0.2593	0.2582
	0.625	0.0043	0.7326	---	0.6027	0.1894	0.1335
	1.25	0.0003	0.9198	0.6027	---	0.0295	0.0070
	2.5	0.0003	0.2593	0.1894	0.0295	---	0.7122
	5	0.0002	0.2582	0.1335	0.0070	0.7122	---

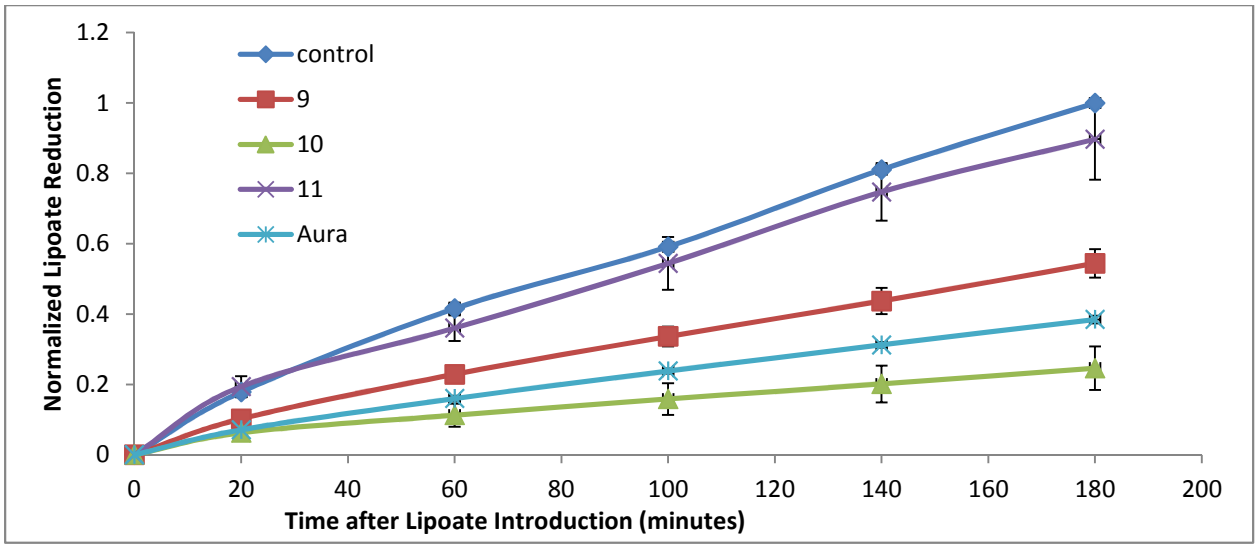

Figure 46. Normalized lipoate reduction with standard error in A549 over 3 hours, after 6 hours incubation in 2.5 µM compound.

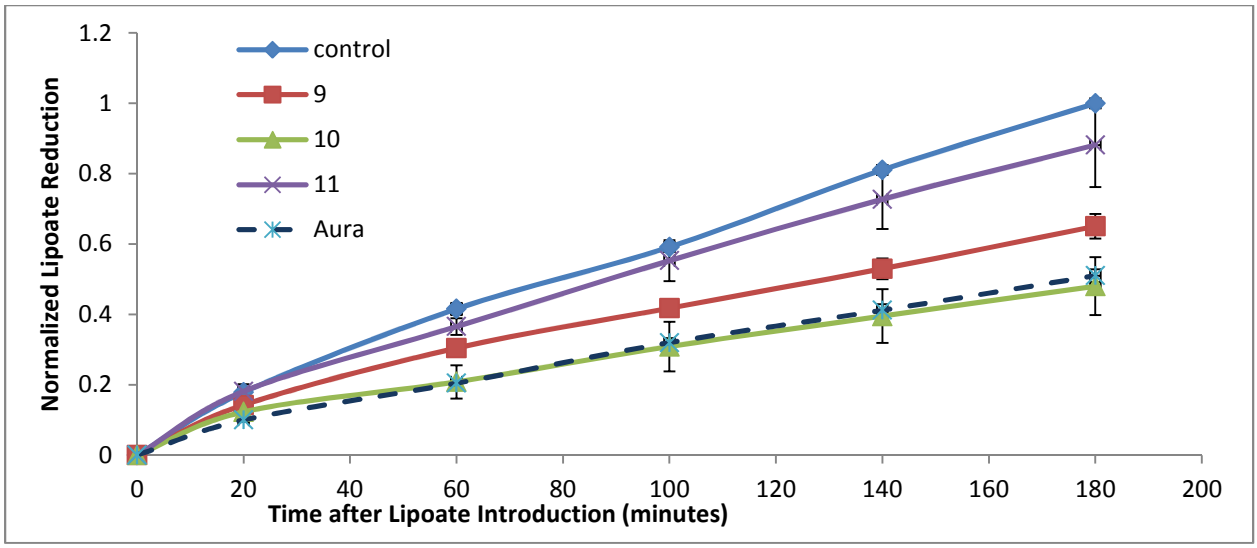

Figure 47. Normalized lipoate reduction with standard error in A549 over 3 hours, after incubation in 1.25 µM compound.